Asian Journal of Chemistry; Vol. 38, No. 6 (2026), 1367-1385
ASIAN JOURNAL OF CHEMISTRY
https://doi.org/10.14233/ajchem.2026.35620

REVIEW

Recent Developments in ZnS-based Hybrid Nanocomposites for Multifunctional Applications in Photocatalysis, Energy and Sensing

SANGRAM KESHARI SAHU and DOJALISA SAHU*

School of Applied Sciences, Centurion University of Technology and Management, P.O. Jatni, Bhubaneswar-752050, India

*Corresponding author: E-mail: dojalisa.sahu@cutm.ac.in

Received: 20 January 2026 *Accepted*: 16 April 2026 *Published online*: 31 May 2026 AJC-22363

Nanocrystalline ZnS-based hybrid nanocomposites have emerged as a versatile class of wide bandgap semiconductor materials with growing relevance in multifunctional applications including photocatalysis, energy conversion and storage and chemical sensing. Their tunable physico-chemical properties, coupled with structural adaptability, have enabled their integration into diverse technological platforms spanning environmental remediation, renewable energy systems and advanced sensing devices. The intrinsic merits of ZnS, such as favourable band-edge positions, high chemical stability and strong redox capability, render it an attractive material for photocatalytic processes. Nevertheless, its wide bandgap and rapid recombination of photogenerated charge carriers severely limit visible-light utilisation and overall performance. To address these challenges, substantial progress has been achieved through compositional doping, defect engineering, surface functionalisation and the rational construction of heterojunction and hybrid architectures. This review systematically summarizes the structural features, charge-transfer mechanisms and recent developments in ZnS-based hybrid nanocomposites, with particular emphasis on strategies for enhancing visible-light absorption, charge-carrier separation and interfacial reaction kinetics. In addition to a detailed discussion on photocatalytic processes, particular attention is devoted to the role of ZnS hybrids in energy-related applications including photoelectrochemical systems, supercapacitors and batteries, as well as their performance in chemical and biological sensing platforms. The interrelationship between structural design, electronic properties and multifunctional performance across these domains is also highlighted to provide a unified perspective. Finally, current challenges, performance bottlenecks and future research directions are outlined to guide the design of next-generation ZnS-based hybrid nanomaterials with improved efficiency, durability and multifunctionality.

Keywords: ZnS, Nanocomposites, Photocatalysis, Green energy, Sensing, Remediation.

INTRODUCTION

The rapid industrialisation and urbanisation of modern society have intensified the demand for sustainable energy and environmental purification technologies [1-5]. The conventional energy resources and chemical processes often generate vast quantities of pollutants and greenhouse gases, leading to serious ecological imbalance [6]. The uncontrolled discharge of industrial effluents, including dyes, pharmaceuticals and toxic organic compounds, has emerged as a critical environmental concern, necessitating the development of efficient remediation strategies. In this context, semiconductor-based photocatalytic materials have evolved as a prospective strategy for addressing global challenges in environmental decontamination [2,3,7-11]. Photocatalysis utilizes light energy to drive oxidation–reduction reactions, enabling the degradation of organic contaminants, water splitting for hydrogen generation and reduction of carbon dioxide into fuels [3,7-9,12-14]. In addition to the environmental concerns, the growing global energy demand and depletion of fossil fuel resources have accelerated research into sustainable energy conversion and storage technologies [15]. Semiconductor materials capable of harnessing solar energy for hydrogen production, as well as their integration into photoelectrochemical cells and energy storage devices, have attracted significant attention [16-19]. Further, the increasing need for real-time monitoring of environmental pollutants and biological analytes has driven advancements in sensing technologies. Semiconductor nanomaterials, owing to their high surface area, tunable electronic properties and sensitivity to surface interactions, have shown immense

potential in chemical and biological sensing applications [20,21]. The ability to detect low concentrations of gases, toxins and biomolecules with high selectivity is crucial for environmental safety and healthcare applications [21,22]. These challenges in environmental remediation, energy sustainability and sensing technologies have stimulated the development of multifunctional materials, which can simultaneously address multiple application domains [23]. In this regard, hybrid nanocomposites have emerged as a promising class of materials, where the synergistic combination of different components and dopants enables enhanced performance through improved charge transfer, extended light absorption and optimised interfacial interactions.

Among various semiconductor materials, ZnS occupies a special position due to its abundance, chemical inertness, non-toxicity and suitable band edge potentials for both oxidation and reduction processes [24-27]. ZnS possesses a wide bandgap energy ranging from 3.4 to 3.8 eV depending on its crystal phase, which allows it to absorb ultraviolet radiation efficiently [27-29]. The conduction band edge of ZnS is sufficiently negative to facilitate the hydrogen evolution reaction, while the valence band edge is positive enough to oxidize water and organic molecules [30,31]. These properties render ZnS thermodynamically capable of participating in a wide array of redox reactions. Although ZnS exhibits several favourable characteristics, its practical photocatalytic performance is constrained by two fundamental issues [32-36]. First, the inherently large bandgap confines its optical absorption primarily to the ultraviolet domain (5% of solar radiation). Second, the quick recombination of photo-induced charge carriers substantially hampers the quantum efficiency during photocatalytic processes [28,29]. To mitigate these intrinsic shortcomings, extensive research has focused on diverse modification approaches such as metal or non-metal ion doping, formation of heterojunctions with semiconductors possessing narrower bandgaps, surface integration with carbonaceous materials and morphological tailoring to regulate particle size and surface area [1,2,31-36]. These strategies are designed to broaden the light-harvesting capacity of the photocatalyst towards the visible spectrum, facilitate more effective charge carrier separation and ultimately strengthen its comprehensive catalytic performance and durability.

In recent years, ZnS-based nanocomposites have gained considerable attention due to their enhanced photocatalytic activity under UV-Vis light and solar irradiation [1,2,37-46]. By combining ZnS with other semiconductors such as TiO_2, CdS, *g*-C_3N_4, ZnO or MoS_2 as well as conductive materials like graphene oxide and carbon nanotubes, synergistic effects have been achieved that improve the utilisation of visible light and facilitate charge migration [1,2,31,32]. Furthermore, doping with transition metals such as Ni, Co and Cu has been shown to tune the band structure and develop mid-gap states for improved photoresponse [32,47-52]. Recently, rapid progress has been occurred in the synthesis of ZnS-based nanocomposites for different applications [53-56]. Innovative fabrication techniques have enabled precise control over crystal phase, morphology and defect distribution, while advanced characterisation tools such as photoluminescence spectroscopy, electrochemical impedance spectroscopy and density functional theory modelling have provided deep insights into the underlying photocatalytic mechanisms [27,57-59]. Moreover, new application fields such as CO_2 photo-reduction and N_2 fixation have emerged, expanding the functional versatility of ZnS nanocomposites [32,60-62]. ZnS-based nanomaterials have also been explored for energy conversion and storage systems, where their semiconducting nature and tunable electronic properties play a decisive role [38,41,43,63,64]. For instance, ZnS-based hybrids have been incorporated into photoelectrochemical cells for solar-driven hydrogen generation, where efficient charge separation and favourable band alignment enhance photoresponse and stability [65-67]. Similarly, ZnS has been investigated as an electrode material in supercapacitors and lithium-ion batteries, where its high theoretical capacity, coupled with nanostructuring and composite formation, improves charge storage capability and cycling stability [63-67].

The integration of ZnS with conductive matrices such as graphene, carbon nanotubes and metal oxides has been shown to significantly enhance electrical conductivity and ion transport kinetics, thereby improving the device performance. ZnS-based nanocomposites have also demonstrated remarkable potential in sensing technologies, including gas sensing, biosensing and environmental monitoring [68-71]. The high surface-to-volume ratio, surface defect states and tunable band structure of ZnS enable sensitive detection of various analytes such as toxic gases, heavy metal ions and biomolecules [38,70,71]. In particular, heterostructured ZnS systems and doped variants exhibit enhanced sensitivity, selectivity and response recovery characteristics due to improved charge transfer and surface adsorption properties [68-71]. Furthermore, the incorporation of ZnS into hybrid sensing platforms has enabled the development of multifunctional sensors with improved stability and real-time detection capabilities, making them suitable for practical environmental and biomedical applications [68,69]. Apart from the aforementioned applications, ZnS-based materials have demonstrated significant potential across a broad spectrum of emerging fields, including the degradation of antibiotics [72], dye-sensitised solar cells [65-67,73], photodynamic therapy [74], bio-imaging [75], biomass valorisation [76,77], solar-driven organic transformations [78,79], CO_2 photoreduction [31,80], selective oxidation-reduction processes [81,82] and photo-assisted redox catalysis [27,73]. These diverse applications underscore the multifunctional nature of ZnS-based nanomaterials and highlight their versatility beyond conventional photocatalytic systems. The continuous expansion of their application domains reflects the adaptability of ZnS through structural modification, compositional tuning and interface engineering, making it a promising candidate for next-generation sustainable technologies. The application landscape of ZnS and ZnS based hybrid materials are schematically illustrated in Fig. 1. In light of these developments, there is a growing need for a comprehensive and critically structured review that integrates advancements in photocatalysis, energy and sensing within a unified framework of ZnS-based hybrid nanocomposites.

Despite significant progress in ZnS-based materials, existing reviews largely focus on isolated aspects such as synthesis methods, photocatalytic degradation, energy storage, sensing and mechano-optical applications [1,2,27,37-42]. Most

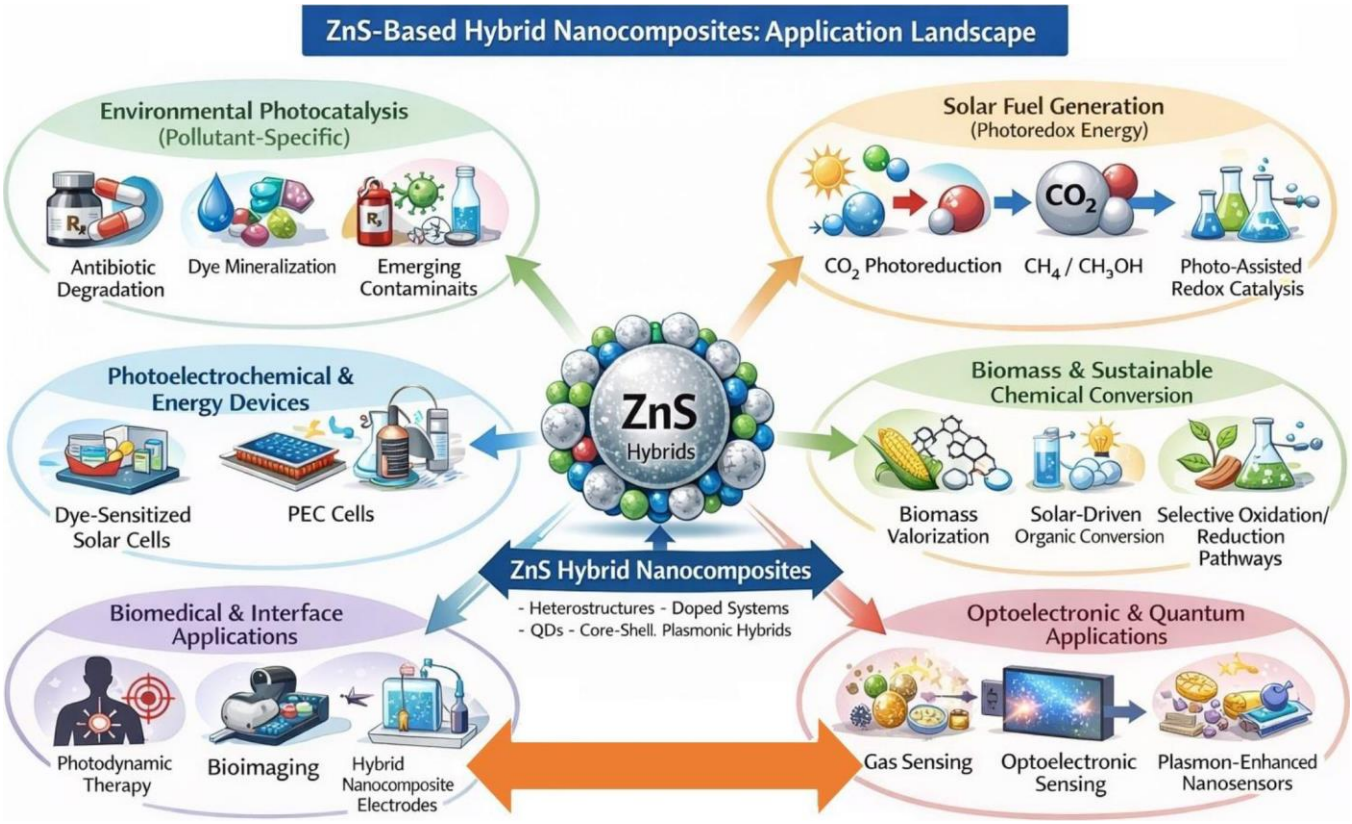

Fig. 1. Application landscape of ZnS-based materials

studies are confined to single domains or emphasize either material properties or device performance without establishing clear correlations between them. Moreover, recent reviews on areas such as supercapacitors, CO_2 conversion and nanogenerators remain fragmented and do not provide a unified perspective on the multifunctional capabilities of ZnS-based systems [1,2,27,37-42]. Khan *et al.* [27] focused specifically on ZnS-based nanoarchitectures for visible-light-driven photocatalytic degradation of antibiotics and organic dyes, but their review remains limited to pollutant degradation and does not address the broader multifunctional applications of ZnS in energy and sensing domains. Although Zhang *et al.* [1] comprehensive reviewed in terms of ZnS quantum dot photocatalysis, remains narrowly focused and does not encompass the broader multifunctional applications of ZnS in energy and sensing domains. In contrast to broader application-oriented studies, Huang *et al.* [39] confined their discussion to mechano-optical functionalities of ZnS, leaving its roles in photocatalysis, energy and sensing unexplored. While Ejeromedoghene *et al.* [42] explored ZnS heterostructures in the context of CO_2 conversion, the study does not integrate insights across photocatalysis, sensing and other application areas. So, a critical gap therefore exists in integrating photocatalysis, energy and sensing within a single coherent framework, particularly for ZnS-based hybrid nanocomposites. This limitation restricts a comprehensive understanding of common design strategies such as doping, defect engineering and binary/ternary heterostructure formation govern performance across multiple applications. In this context, the present review provides a unified and cross disciplinary perspective by correlating structural and compositional modifications with multifunctional performance of ZnS based materials in photocatalysis, energy conversion/storage and sensing. It begins with the structural aspects of ZnS, followed by an analysis of photocatalytic mechanisms including charge generation, transfer and reaction pathways. Subsequent sections discuss nanocomposite design strategies such as doping, defect engineering and hybrid architectures and their roles in enhancing multifunctional performance. Recent developments in photocatalysis, energy and sensing applications are highlighted, along with key challenges and future prospects. Thus, this review provides a clear understanding of the influence of structural, compositional and interfacial modifications on performance and offers guidance for the rational design of advanced multifunctional ZnS-based systems.

Methods: The review methodology was adopted to collect and analyze published studies related to ZnS-based materials. The literature search was conducted using major scientific databases including Scopus, Web of Science and Google Scholar to ensure comprehensive coverage of relevant research articles. The search was performed using combinations of keywords such as “ZnS photocatalyst,” “zinc sulphide photocatalysis,” “ZnS nanostructures,” “ZnS heterojunction photocatalyst,” “ZnS visible-light photocatalysis,” “ZnS-based materials for energy storage”, “ZnS-based materials for sensing” and “ZnS-based nanocomposites for environmental remediation”. The Boolean operators (AND, OR) were used to refine the search results. Only peer-reviewed journal articles published in English were considered. The review focused primarily on publications from 2012 to 2026, covering recent developments in ZnS-based photocatalysts for environmental and energy-related applica-

tions. The initial database search yielded approximately 610 records. After removing duplicate entries, 474 articles remained for further screening.

These articles were screened based on titles and abstracts to determine their relevance to ZnS-based materials. During the screening stage, studies not directly related to ZnS for photocatalysis, energy storage and sensing with overlapping scope, conference abstracts and non-peer-reviewed sources were excluded. After this step, 251 full-text articles were assessed for eligibility. Finally, 229 articles that specifically discussed synthesis methods, structural properties, heterojunction design, photocatalytic mechanisms and applications of ZnS-based photocatalysts were selected for detailed analysis and discussion in this review. The literature identification, screening, eligibility assessment and final study selection process are summarised in the PRISMA flow diagram presented in Fig. 2. This methodology follows the reporting principles recommended by the PRISMA Statement proposed by Moher *et al.* [83] and the updated PRISMA 2020 by Page *et al.* [84]. A graphical representation illustrating the year-wise distribution of selected studies included in this review has been depicted in Fig. 3.

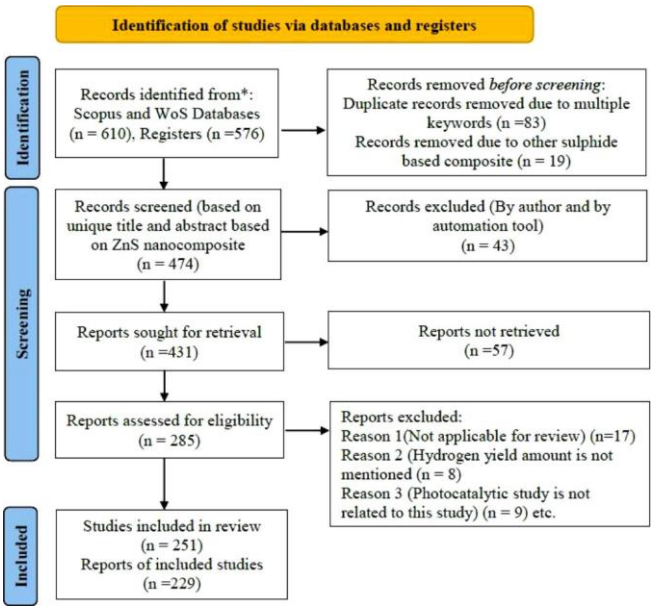

Fig. 2. PRISMA flow diagram for review article on ZnS hybrid nanocomposites and its applications photocatalysis, energy and sensing

Structure and properties of ZnS: Zinc sulphide exists primarily in two crystalline phases; zinc blende (cubic) and wurtzite (hexagonal) both of which consist of tetrahedrally

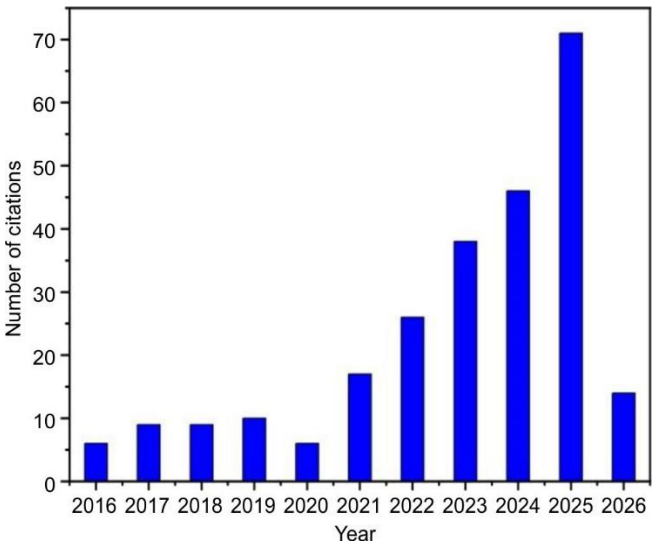

Fig. 3. Illustration showing year-wise literatures reviewed and discussed in this article

coordinated zinc and sulphide atoms [1,2,85]. The cubic zinc blende phase is thermodynamically stable at room temperature, while the wurtzite phase is metastable but can be stabilised at nanoscale dimensions or elevated temperatures [2,86]. The structural difference between these two polymorphs lies in their atomic stacking sequence: ABCABC for zinc blende and ABAB for wurtzite [39]. Despite this variation, both structures share similar bond lengths and coordination geometry, resulting in comparable electronic properties. The electronic configuration of Zn^{2+} ($3d^{10}$) and S^{2-} ($3p^6$) leads to a direct bandgap semiconductor with strong excitonic binding energy [1,2,39]. The conduction band is primarily derived from the 4*s* and 4*p* orbitals of zinc, while the valence band arises from the 3*p* orbitals of sulphide [1,39]. The wide bandgap of ZnS restricts light absorption to the ultraviolet region, but it also contributes to its high redox potential, making it capable of driving both reduction and oxidation processes efficiently. Furthermore, the large bandgap helps prevent photo-corrosion, imparting ZnS with remarkable chemical stability during long-term photocatalytic reactions [2,87,88]. The zinc blende and hexagonal structures of ZnS have been illustrated in Fig. 4 and the structural parameters are summarised in Table-1.

Photocatalytic properties and mechanism of ZnS-based systems

Fundamentals of photocatalysis: In ZnS-based photocatalysts, the initiation of photocatalysis occurs when the semiconductor captures photons possessing energies that

TABLE-1
STRUCTURAL PROPERTIES OF ZNS (ZINC BLENDE & WURTZITE) [1]

ZnS phase	Wurtzite	Zinc blende
Crystal structure	Hexagonal	Cubic
Symmetry	Hexagonal close-packed	Face-cantered cubic
Lattice constants	a = b = 0.382 nm, c = 0.626 nm	a = b = c = 0.541 nm
Space group	P63mc	F-43m
Coordination	Tetrahedral	Tetrahedral
Stability	Stable at T ≥ 1020 °C	Stable at ambient conditions
Band gap	~3.91 eV	~3.68 eV

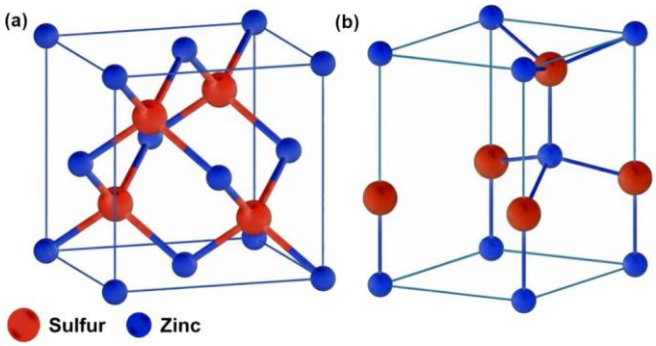

Fig. 4. Polymorphism in zinc sulfide (ZnS): (a) zinc blende structure (cubic phase) and (b) wurtzite structure (hexagonal phase) [1]

meet or surpass its bandgap [89-92]. This photon absorption drives the transition of electrons from the valence band to the conduction band, resulting in the development of electron-hole pairs (eqn. 1) [2,90]. Following this excitation, the photo-generated charges move toward the surface of the catalyst, where they actively participate in redox reactions (eqn. 2) [1,2,93,94]. Specifically, the photogenerated electrons are capable of reducing hydrogen ions or molecular oxygen (eqn. 3) to form $^{\bullet}O_2^-$, whereas the corresponding holes facilitate the oxidation of organic substrates or water molecules, leading to the generation of hydroxyl radicals ($^{\bullet}OH$) (eqn. 4) [95-99]. This reactive oxygen species ($^{\bullet}OH$ and $^{\bullet}O_2^-$) play a great role to perform a redox reaction on the surface of catalyst along with the pollutant present in the water to form various oxidizes and reduced product along with water and carbon dioxide (eqn. 4). The steps of reaction mechanism involved in the photocatalytic processes are summarised below [100-110].

Photoexcitation involves the excitation of catalyst with photon of light:

$$\text{Photocatalyst} + h\nu \rightarrow eCB^- + h_{VB} \quad (1)$$

Electron hole-recombination:

$$e_{CB}^- + h_{VB}^+ \rightarrow \text{Heat} \quad (2)$$

Production of superoxide anion radical:

$$O_2 + e_{CB}- \rightarrow {}^{\bullet}O_2^- \quad (3)$$

Production of hydroxyl radical:

$$H_2O + h_{VB}^+ \rightarrow {}^{\bullet}OH + H^+ \quad (4)$$

Degradation processes:

Organic dye (pollutant) + $^{\bullet}OH \rightarrow$ Degradation products

Pollutant + $h_{VB}^+ \rightarrow CO_2 + H_2O$ + Oxidised products (5)

Pollutant + e_{CB}- $\rightarrow CO_2 + H_2O$ + Reduced products

The favourable positioning of the conduction and valence band potentials relative to standard redox levels endows ZnS with adequate thermodynamic capacity to facilitate both oxidation and reduction reactions effectively [95,111-115]. This coordinated charge migration and redox reaction pathway underpin the overall photocatalytic activity of ZnS, as summarised in the schematic (Fig. 5) [116-118].

Charge generation and transfer dynamics: When ZnS absorbs light, the electrons excited to the conduction band gain sufficient energy to initiate reduction reactions [15,16,95]. At the same instance, holes left behind in the valence band

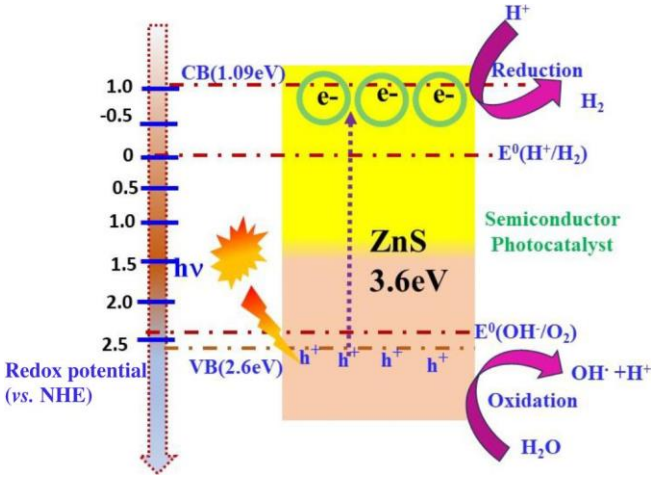

Fig. 5. Schematic illustration of the photocatalytic mechanism in ZnS under light irradiation [116]

possess strong oxidizing potential [110-116]. The photocatalytic process depends on the balance among charge generation, migration, and recombination [111-117]. Surface adsorption of reactants is also a critical step, as it determines the probability of charge transfer from the semiconductor to the adsorbed molecules [40,119]. The valence band edge potential of the semiconductors can be estimated from their bandgaps (E_g), the electronegativity (χ) and the energy of free electrons *versus* a normal hydrogen electrode (NHE) (E = 4.5 eV) using eqn. 6. The conduction (CB) and valence band (VB) edge positions of the semiconductor photocatalysts were estimated using standard equations as given below:

$$E_{VB} = X - E_0 + 0.5E_g \quad (6)$$

$$E_{CB} = E_{VB} - E_g \quad (7)$$

where E_{VB} shows the valence band potential and E_{CB} states to the conduction band potential. E_g implies the band gap energy and its value ranges from 3.02 to 3.6 eV for ZnS [2,40,119]. The electronegativity (χ) of the semiconductor (5.21 eV for ZnS) and E_0 is the energy of free electrons on the hydrogen scale (4.43 eV) [40,119]. The electronegativity of a semiconductor with two number of compounds *i.e.* a and b are of A and B respectively, can be found from the following equation:

$$\chi = [(A)^a \times (B)^b]^{1/(a+b)} \quad (8)$$

Based on these parameters, the valence and conduction band positions can be calculated for ZnS. Nanostructured ZnS materials with high surface areas and suitable surface functionalities provide abundant active sites for adsorption and reaction. However, the presence of surface defects and dopants modifies the local electric field and potential barriers, facilitating faster migration of charge carriers to reactive sites [40,95,119,120]. The use of conductive supports such as graphene or carbon nanotubes further enhances charge mobility and prevents accumulation of charges that lead to recombination [120,121].

Role of band structure and energy alignment: The photocatalytic performance is primarily governed by how the conduction and valence band edge positions align with the redox potentials of the specific reactions involved [122]. ZnS possesses a highly negative conduction band, enabling efficient reduction of protons to hydrogen gas [123-127]. Its valence

band is sufficiently positive to oxidize water and organic compounds, making ZnS an excellent dual-function photocatalyst [95]. However, its wide bandgap limits visible-light absorption. To extend photoresponse into the visible region, researchers have employed bandgap engineering through doping and heterojunction construction [101,128-130]. Doping introduces impurity levels within the bandgap, allowing lower-energy photons to excite electrons [121].

Zinc sulphide can be effectively modified through various strategies such as metal deposition, non-metal doping and dye sensitisation to mitigate its inherent limitations [131]. For efficient photocatalytic redox reactions, it is essential that the conduction band and valence band potentials of the semiconductor are suitably aligned with the redox potentials of the targeted reactions. Fig. 6 illustrates the band edge positions, including the CB and VB levels, of selected semiconductors that are considered promising candidates for reactive oxygen species (ROS) generation. As illustrated in Fig. 6, the CB potential of ZnS (-1.36 eV *vs.* NHE) is significantly more negative than the H^+/H_2 redox potential (0 eV *vs.* NHE), whereas its VB potential (+2.35 eV *vs.* NHE) is more positive than the O_2/H_2O oxidation potential (1.23 eV *vs.* NHE) [1,2]. This favourable band alignment indicates that ZnS is thermodynamically suitable for photocatalytic water splitting and hydrogen generation. In addition, the highly reducing electrons in the CB of ZnS can promote the conversion of CO_2 into value added hydrocarbon products such as CO, CH_3OH and CH_4, while the photogenerated holes in the VB can oxidise water to generate O_2 [132]. The highly negative CB and strongly positive VB potentials account for the excellent reduction and oxidation capabilities of ZnS, respectively. However, the relatively wide bandgap of ZnS (3.68 eV) restricts its absorption primarily to the ultraviolet region, corresponding to only about 5% of the solar spectrum [133,134]. Therefore, broadening the light absorption range of ZnS is crucial to enhance its overall photocatalytic performance. Heterojunctions, on the other hand, combine two semiconductors with different band structures, enabling charge transfer across their interface and efficient utilisation of visible light [1,2,41,42,128-138].

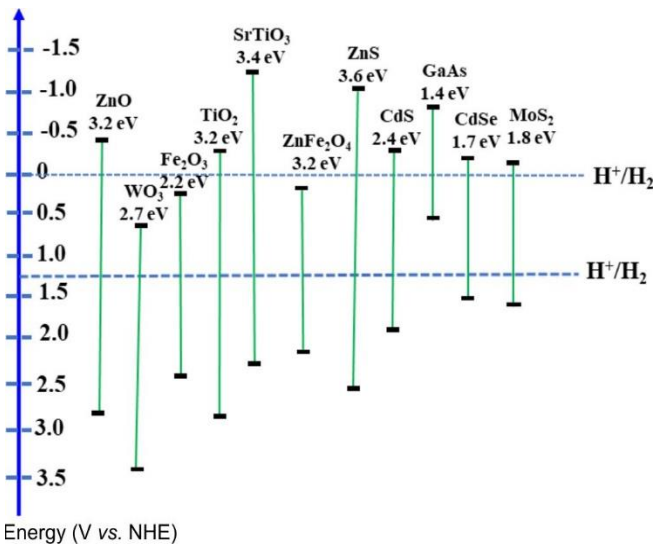

Fig. 6. Band-edge positions of selected semiconductors *vs.* the normal hydrogen electrode (NHE) [1,2]

Enhancement strategies

Doping and defect engineering: Doping of ZnS with transition metals (*e.g.*, Ni, Co, Mn, Cu) has proven to be an effective approach to modify its optical and electronic properties [47,103-107]. Metal doping introduces discrete energy states within the bandgap, enhancing visible-light absorption and reducing recombination by acting as charge traps [31, 139-143]. Non-metal doping, particularly with nitrogen or carbon, creates shallow acceptor levels near the valence band edge, thereby narrowing the effective bandgap [144,145]. Defect engineering, which involves the controlled creation of sulphide vacancies or zinc interstitials, also plays a crucial role in tailoring photocatalytic performance. These defects act as active centers for charge trapping, improving charge separation and extending light absorption [1,2]. However, excessive defect concentrations may introduce deep traps that accelerate non-radiative recombination [47]. Therefore, optimizing defect density is vital to achieving maximum efficiency.

When ZnS is doped with transition metal ions (M^{n+}), new electronic states are introduced within the bandgap [145-148]. M^{n+} as dopant ions generate discrete trap levels that serve as intermediate energy states, capturing photogenerated charge carriers and thereby minimizing direct recombination [2]. These trapped electrons are gradually transferred to surface-active sites, where they reduce adsorbed oxygen molecules to superoxide radicals ($O_2^{\bullet-}$) [1,2]. Meanwhile, photogenerated holes migrate to the surface, oxidizing water or hydroxide ions to form reactive hydroxyl radicals ($^{\bullet}OH$) [149-151]. This dopant-mediated charge separation significantly extends carrier lifetimes and enhances redox efficiency, leading to superior photodegradation efficiency under light of visible range [1,2]. The band diagram (Fig. 7) highlights the interaction between the metal dopant states and the intrinsic electronic structure of ZnS, emphasizing the role of defect and dopant engineering in tuning its photocatalytic properties.

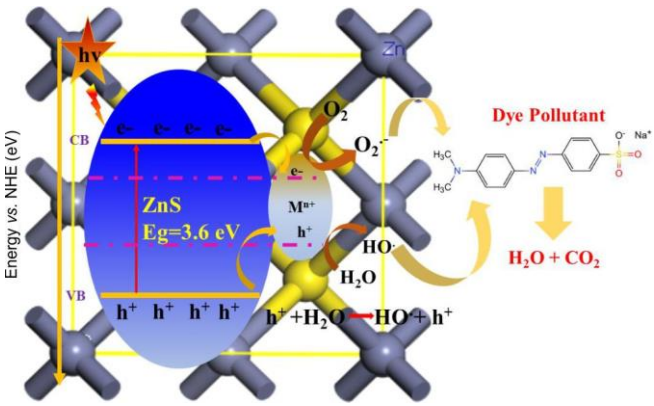

Fig. 7. Schematic representation of the photocatalytic enhancement mechanism in metal-ion-doped ZnS [145,146]

Heterojunction construction: Heterojunctions are among the most effective architectures for enhancing charge separation and extending light absorption [152-156]. In type-II heterojunctions (Fig. 8a), the conduction band of one semiconductor lies at a higher energy level than that of the other semiconductor, facilitating directional electron flow [155-157]. When ZnS is coupled with semiconductors such as TiO_2 or *g*-C_3N_4,

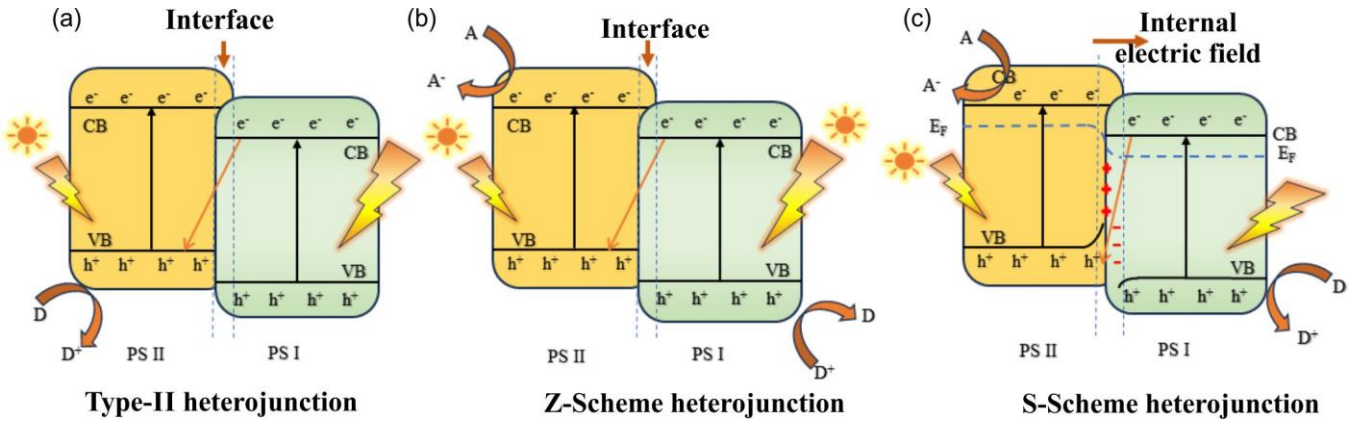

Fig. 8. Different types of heterojunctions for enhancing charge separation [1]

electrons transfer from the lower to the higher conduction band and holes move in the opposite direction, minimizing recombination [16,158-169]. Dong *et al.* [159] reported the ZnS-Bi-TiO_2 nanocomposite formation by sol-gel method, where Bi as Bi^{4+}/Bi^{3+} species enhance the light absorption ability of TiO_2 lattice in visible region and reduced the recombination of photogenerated electrons and holes [159]. After incorporation of ZnS (0.005 M) to Bi-TiO_2 (Bi/Ti = 0.006), sulphur doping into the lattice reduced the band gap energy, thereby increasing the catalytic efficiency. In Z-scheme heterojunctions (Fig. 8b), photogenerated electrons in one semiconductor recombine with holes in another, preserving the high redox potential of both charge carriers [158,170-173]. This mechanism mimics natural photosynthesis and has been particularly successful in ZnS-QDs@$CoWO_4$, Fe_2O_3@BNP @ZnS/CdS and ZnS/MoS_2 composites [134,174-177].

Zhang *et al.* [174] described the fabrication of Z-scheme heterostructures of ZnS quantum dots wrapped around $CoWO_4$ nanoparticles (ZnS-QDs@$CoWO_4$) as shown in Fig. 9. In this work, an optimal catalyst dosage of 25 mg of nanocomposite exhibited the highest photocatalytic activity toward the degradation of tetracycline hydrochloride (TC·HCl), achieving a rate constant (k = 0.03427 min^{-1}). This value is approximately 3.5 times higher than that of ZnS quantum dots (k = 0.00969 min^{-1}) and nearly 214 times greater than that of $CoWO_4$ (k = 0.00016 min^{-1}). The superior photocatalytic performance can be attributed to the formation of a Z-scheme heterojunction within the composite system, which effectively enhances charge separation while preserving strong redox potentials of the photogenerated charge carriers [174]. A comparable trend has been reported by Khodamorady *et al.* [175] where 0.08 g of Fe_2O_3@BNP@ZnS/CdS nanocomposite achieved 98% degradation of methylene blue and 68-100% removal efficiency for various textile dyes under 90 min of visible light irradiation. Recently, enhanced photocatalytic degradation efficiency of ZnS toward rhodamine B has been reported through the formation of a Z-scheme heterojunction with MoS_2 in ZnS-MoS_2 nanocomposites [134].

Fig. 10 demonstrates the band alignment and interfacial charge transfer process in ZnS coupled with a secondary semiconductor, such as a metal oxide or metal sulphide. Upon illumination, both semiconductors absorb photons, generating electron-hole pairs [4-6]. Rashid *et al.* [178] highlighted the

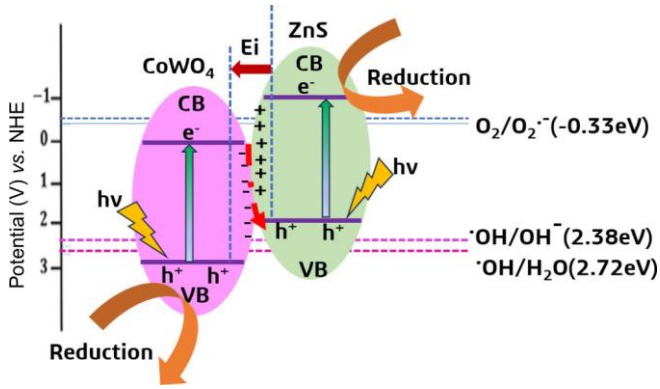

Fig. 9. Schematic diagram of charge transfer mechanism in ZnS–QDs @ $CoWO_4$ direct Z-scheme heterojunction [138]

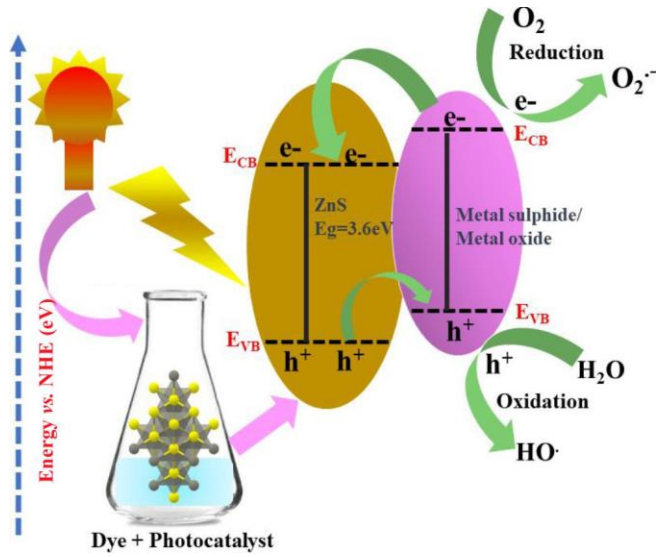

Fig. 10. Schematic illustration of charge transfer and photocatalytic mechanism in ZnS-based heterojunctions

degradation of 2,4,6-trichlorophenol by WO_3/ZnS using various illuminating sources *i.e.* solar, UV/visible light. In the above study, ZnS was coupled with WO_3 as it is a stable, economic and photo-corrosion resistant material with relatively lower band gap of 2.4 eV-2.8 eV. The degradation efficiency was found to be 65% initiated by the reactive oxygen species ($^{\bullet}OH$, $^{\bullet}O_2^-$), electron with first order kinetics having maxi-

mum rate of 0.0249 min^{-1}. The degradation mechanism followed a direct Z-scheme heterostructure for charge transfer without the involvement of any mediator but due to creation of an in-built electric field, established between two adjacent photosystems, correspondingly. Behin *et al.* [179] synthesised ZnS/ZnO nanocomposites for photocatalytic degradation of Congo red in textile wastewater, achieving 91% removal efficiency at a catalyst loading of 0.4 g L^{-1}. Band structure (Fig. 11a) analysis revealed a reduction in bandgap from 3.70 eV (pristine) to 3.46 and 3.41 eV for the ZnS/ZnO composite, confirming the formation of a type-II heterojunction. This band alignment enhances visible-light absorption and promotes efficient charge separation, resulting in improved photocatalytic performance. The degradation follows pseudo-first-order kinetics with a rate constant of 0.027 min^{-1}. Dong *et al.* [180] successfully synthesised MoS_2/ZnCdS/ZnS dual heterostructures. The synergistic coupling of these multiple semiconductors significantly enhanced the photocatalytic hydrogen evolution performance, achieving a rate of 79.3 mmol g^{-1} h^{-1} under visible-light irradiation, along with an apparent quantum efficiency of 47.9% at 420 nm in the absence of noble-metal co-catalysts. This activity is approximately fivefold higher than that of the MoS_2/ZnCdS system (15.7 mmol g^{-1} h^{-1}) and about nine-fold greater than that of the ZnCdS/ZnS counterpart (8.98 mmol g^{-1} h^{-1}) and shown in Fig. 11b. Hence, the coupling of ZnS with other semiconductors thus provides an efficient pathway for improved charge separation, broader light absorption and enhanced photocatalytic performance [92,175-181].

Photocatalytic applications

Degradation of organic pollutants: Among the various applications of ZnS-based photocatalytic materials, one of the most extensively explored is the removal of organic contaminants such as dyes, antibiotics and phenolic derivatives [1-7]. The complete degradation performance is strongly influenced by intrinsic material properties such as specific surface area, degree of crystallinity and the presence of structural defects [7,92]. ZnS-based composites with hierarchical structures and optimised band alignment exhibit remarkable degradation rates even under visible light [92,157,167]. Addition of ZnS to TiO_2 improves the separation of photogenerated electron-hole pairs and extends the absorption range to the visible light region. As reported, nanostructured ZnS/TiO_2 synthesised by chemical deposition technique removed 99.0% of acid blue, an industrial diazo dye under UV light [158, 182]. Another study also reported a similar trend. Talebi *et al.* [160] demonstrated that ZnS/TiO_2 nanocomposites achieved up to 99% degradation of acid blue 113 dye under optimised conditions. Maximum photocatalytic efficiency was obtained using a low catalyst dosage (37 mg) at pH 6.18 within 27.32 min, outperforming the individual ZnS and TiO_2 counterparts [124]. The introduction of carbon-based supports and transition-metal dopants further enhances degradation kinetics and extends catalyst durability [183,184]. Vignesh & Kim [184] reported a carbon-based ZnS hybrid system comprising highly dispersed Co_3O_4 grown on *g*-C_3N_4 (GCN), coupled with ZnS quantum dots as interfacial bridges *via* a facile hydrothermal route. The Co_3O_4 and ZnS QDs establish robust interfacial bonding with GCN, facilitating efficient charge transport, suppressing nanoparticle agglomeration and generating abundant catalytic active sites for hydrogen evolution. The GCN/Co_3O_4/ZnS heterostructure exhibited 93.05% photo-degradation efficiency toward RhB under light irradiation. Based on eqns. 6 and 7, the conduction and valence band edge potentials were estimated as –1.115 and 1.595 eV for GCN, 0.278 and 2.528 eV for Co_3O_4 and –1.16 and 2.65 eV for ZnS (*vs.* NHE), respectively. These band alignments support a Z-scheme charge transfer mechanism governing RhB degradation over the GCN/Co_3O_4/ZnS heterostructure (Fig. 12) [184].

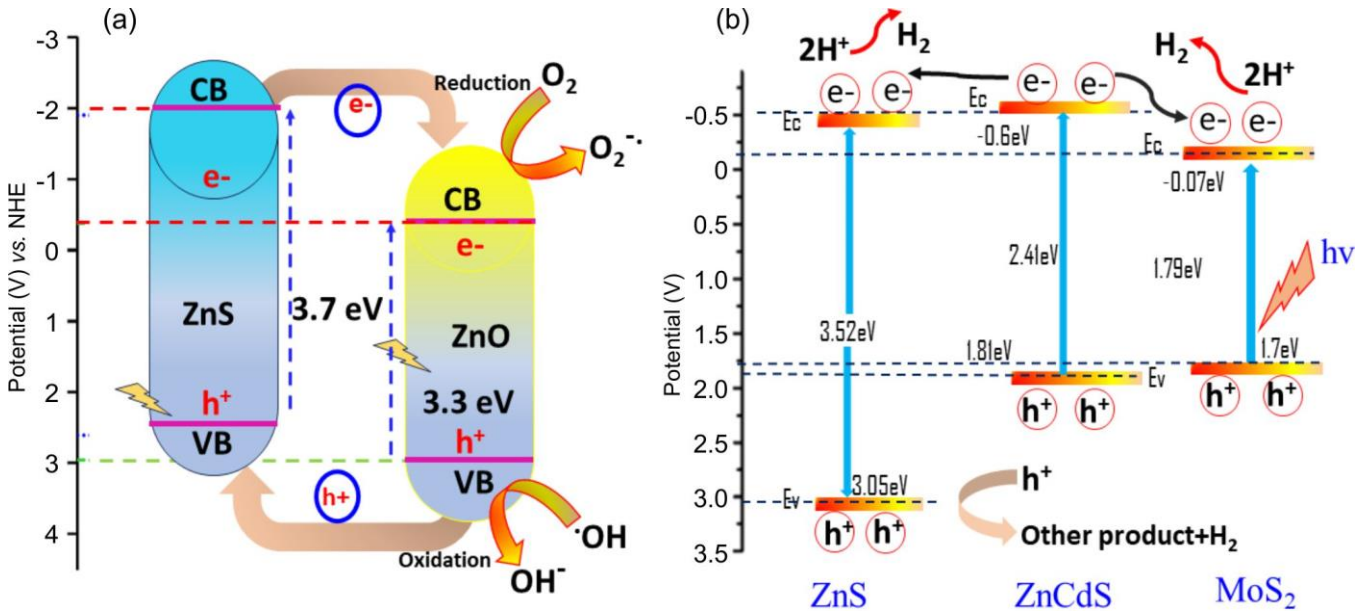

Fig. 11. Schematic illustration of charge transfer and photocatalytic mechanism in ZnS-based Type-II heterojunctions (a) ZnS/ZnO nanocomposites [179], (b) energy band alignment, interfacial charge-transfer-pathways and photocatalytic H_2 evolution mechanism in MoS_2/ZnCdS/ZnS dual heterostructures [181]

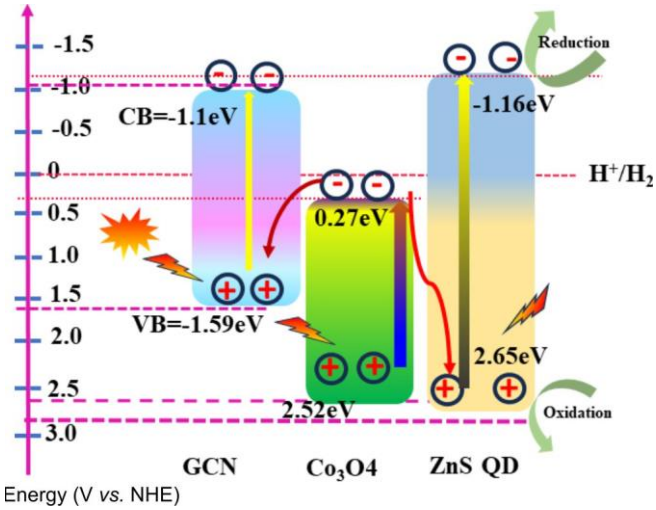

Fig. 12. Energy band alignment and proposed photocatalytic degradation mechanism of as-synthesised ternary GCN/Co_3O_4/ZnS heterostructure under light irradiation [184]

Coupling ZnS with 2D materials such as graphene oxide, MXenes and GCN has been shown to facilitate interfacial charge transfer and suppress electron-hole recombination, thereby improving degradation efficiencies under solar or visible-light irradiation [167,185-188]. Chen *et al.* [186] synthesised a porous ZnS/MXene (Ti_3C_2) nanocomposite *via* a one-step hydrothermal route, in which layered Ti_3C_2 MXene functions as an efficient cocatalyst. The composite exhibited 96% degradation of tetracycline hydrochloride (TCH·HCl) within 60 min under simulated solar irradiation. Additionally, ZnS-based photocatalysts have demonstrated high efficiency in degrading emerging contaminants such as pharmaceutical residues (tetracycline, ciprofloxacin) and endocrine-disrupting chemicals, marking their relevance for next-generation wastewater treatment [92].

Sustainability aspects have also gained attention, where ZnS-based nanocomposites synthesised through green routes such as plant extract-assisted, hydrothermal or sol-gel methods have shown not only improved degradation performance but also higher recyclability and minimal leaching [92]. The integration of magnetic components (*e.g.* Fe_3O_4/ZnS composites) enables easy recovery of the catalyst using external magnetic fields, addressing a key limitation in large-scale photocatalytic systems [189]. These developments highlight the significant potential of rationally engineered ZnS-based nanostructures for efficient and sustainable degradation of diverse organic pollutants. Strategies involving defect engineering, heterojunction formation and surface modification play crucial roles in enhancing photocatalytic efficiency and stability [92]. Table-2 shows a summary of degradation performance of ZnS based materials in decomposing various pollutants. It shows the effective mineralisation ability of ZnS and ZnS based hybrid nanocomposites towards many dye pollutants and antibiotics.

Applications of ZnS in energy production and storage

Reduction of carbon dioxide (CO_2): The escalating global energy demand and increasing environmental concerns associated with carbon emissions have intensified research efforts toward the conversion of CO_2 into sustainable fuels and value-added chemicals [42]. Processes such as hydrogenation and reforming enable the transformation of CO_2 into products including CH_4, CO, formic acid, olefins and CH_3OH, offering viable alternatives to conventional fossil-based resources. Fig. 13 shows the transformation of CO_2 into renewable energy and chemical compounds [42]. ZnS-based nanocomposites have also shown potential in photocatalytic CO_2 reduction to produce value-added fuels such as CO, CH_4 and methanol [7,30,42,208-211]. The process involves the activation of CO_2 molecules adsorbed on the catalyst surface, followed by multi-electron reduction pathways facilitated by photogenerated electrons [30,42]. ZnS based nanocomposites have demonstrated selective reduction of CO_2 with enhanced efficiency under visible light [30,42]. These materials exhibit favourable electronic structures, tunable optical properties and appropriate conduction band potentials, enabling efficient activation and reduction of CO_2 into value-added products. Their ability to facilitate charge separation and transfer further enhances catalytic performance in CO_2 conversion processes. Nam *et al.* [212] demonstrated that a ZnS electrocatalyst achieves 83% CO Faradaic efficiency with suppressed hydrogen evolution, highlighting its effectiveness for selective and stable CO_2 electro-reduction. Luo *et al.* [213] demonstrated that hexagonal phase ZnS exhibits significantly enhanced CO_2 reduction selectivity (21% CO) compared to cubic ZnS (0.2%), attributed to its more negative conduction band and favourable intermediate adsorption characteristics. So, tailoring the structural and electronic properties of ZnS is crucial for steering CO_2 reduction pathways, offering a promising route towards selective and efficient photocatalytic carbon conversion systems.

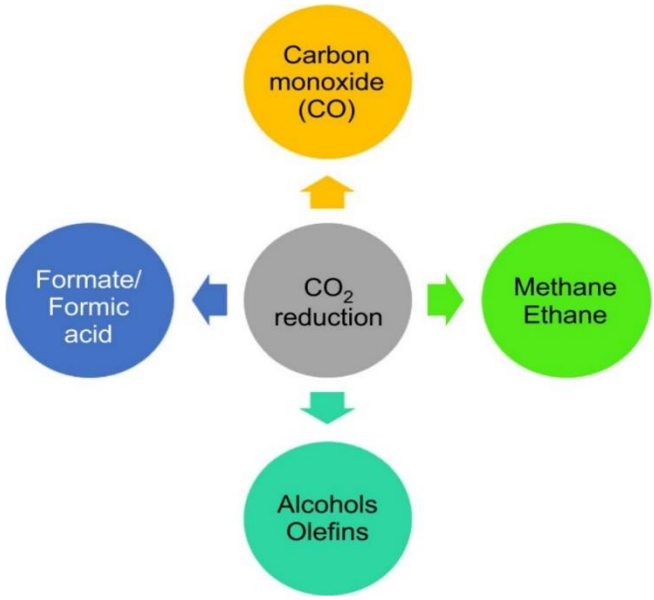

Fig. 13. Transformation of CO_2 leading to chemical compounds and renewable energy sources [42]

Hydrogen evolution reaction (HER): The photocatalytic hydrogen evolution reaction is a key step towards achieving solar-driven water splitting for clean fuel production [18,188,214-218]. ZnS, with its negative conduction band potential,

TABLE-2
RECENT STUDIES ON THE PHOTOCATALYTIC PROPERTY OF ZnS AND ZnS BASED MATERIALS

Name of material	Method of preparation	Name of pollutant	Degradation efficiency (%)	Catalyst dose	Reaction condition	Rate constant (k)	Ref.
ZnS-TiO_2	Solvothermal + wet-chemical	Benzyl alcohol	89.1	200 mg/L	Xenon Lamp 300 W, 5 h	-	[25]
ZnS/Ag_2WO_4	Co-precipitation	Methylene blue (MB) (10 mg/L)	84	3 mg/L	800 W halogen lamp	-	[32]
ZnS-CuSe	Sonochemical	Methylene blue (MB)	98	100 mg/L	400 W visible light, 300 min	1st Order	[33]
ZnS@ZnO	Hydrothermal	Methylene blue (MB)	95.3	100 mg/L	400 W halogen lamp, 300 min	0.0059 min^{-1}	[34]
V_2O_5-ZnS	Co-precipitation	Ciprofloxacin, amoxicillin	96, 94	-	Sunlight simulator lamp (300 W), 200 min	0.021 min^{-1}, 0.029 min^{-1}	[44]
SnO_2/ZnS	Co-precipitation + ultrasonic + hydrothermal	Methyl yellow	89	10 mg/L	36-W LED light, 120 min	0.0263 min^{-1}	[45]
ZnS/PTA	Sonochemical	Rhodamine B (RhB) (10)	78.59	500 mg/L	300 W xenon lamp	0.013 min^{-1}	[46]
ZnS	Hydrothermal	Methylene blue (MB) Alizarin red (AR)	82.12 85.51	5 mg/L	UV light, 180 min	0.0023 min^{-1}	[95]
ZnS/TiO_2	Chemical deposition	Acid blue 113	99	240 mg/L	400 W Kr UV lamp, 30 min	-	[160]
ZnS@*g*-C_3N_4	Chemical method	Acid blue 25	98	4000 mg/L	Sunlight (120 min)	0.010832 min^{-1}	[167]
g-C_3N_4/ZnS	Microwave-assisted	Malachite green (MG)	33.50	30 mg/L	250 W tungsten halogen Lamp, 120 min	0.57 h^{-1}	[168]
ZnS/ZnO	Chemical method	Congo red (CR) (30 mg/L)	98	400 mg/L	UVAB irradiation at 25 ± 2 °C, 120min	0.027 min^{-1}	[179]
ZnS@In_2S_3	Refluxing method	*o*-DCB	49	150 mg/L	visible light (λ > 400 nm), 8 h	0.0538 h^{-1}	[180]
ZnS/MXene Ti_3C_2	Hydrothermal	Tetracycline hydrochloride (TCH) (10 mg/L)	96	100 mg/L	500W metal halide lamp, 60 min	0.0471min^{-1}	[186]
ZnO/*g*-C_3N_4/ZnS	Chemical method	Methylene blue (MB)	80	1000 mg/L	UV lamp 9 W, 90 min	0.02272 min^{-1}	[188]
ZnS	Precipitation	Methylene blue (MB) (2.6)	61	100 mg/L	1000 W tungsten–halogen lamp, 180 min	4.9×10^{-3} min^{-1}	[190]
ZnS	Hydrothermal	Methylene blue (MB) (12)	92	100 mg/L	UV light, 200 min	-	[191]
ZnS	Sulfuration with precipitation	*p*-Nitro phenol (PNP) (10)	51	150 mg/L	UV-LEDs 12 W, 365 nm, 240 min	-	[192]
ZnS	Refluxing followed by calcination	Crystal violet (0.025 mM) 2-Nitrophenol (0.025 mM)	93 88	200 mg/L	Hg arc, 125 W, 300–390 nm, 180 min	0.01649 min^{-1} 0.00366 min^{-1}	[193]
ZnS	Lyotropic liquid crystal template	Methylene blue (MB) (20 mg/L)	99.76	400 mg/L	Xenon lamp 300 W, 350 nm < λ < 780 nm, 150 min	0.040 min^{-1}	[194]
ZnS	Reflux	Methylene blue (MB) (3.2) Methyl orange (MO) (3.27)	96.73 94.68	1000 mg/L	UV-light, 120 min	0.0220 min^{-1}	[195]
ZnS	Hydrothermal	Crystal red (CR) (50)	96.53	200 mg/L	350 W, Hg lamp, 120 min	27.85×10^{-3} min^{-1}	[196]
ZnS	Hydrothermal	Methyl orange (MO) (3.75)	80	700 mg/L	UV-c lamps (253.7 nm, 33.6 µw cm^2) 60 min	0.0315 min^{-1}	[197]
ZnS	Precipitation	Methylene blue (MB) Xylenol orange (XO) Methyl orange (MO) Methyl red (MR) (50)	78.41 81.22 90.90 95.10	500 mg/L	18W visible light, 120 min	0.02052, 0.04380, 0.08310, 0.09469 min^{-1}	[198]
ZnS	Precipitation	Congo red (CR) (30)	98.78	50 mg/L	45 W halogen lamp	-	[199]
ZnS	Hydrothermal	Malachite green (MG)	74.25	–	Solar light, 240min	0.00556min^{-1}	[200]
ZnS/Ag_2O	Precipitation	Methylene blue (MB) (10)	92.4	500 mg/L	300 W xenon lamp (PLS-SXE300 UV	0.138 min^{-1}	[201]
ZnS/$CuFe_2O_4$	Co-Precipitation	Methylene blue (MB) (30) Crystal violet (CV) (30)	82 87	10 mg/L	200 W tungsten halogen light,120min	14.16×10^{-3} sec^{-1} 17.15×10^{-3} sec^{-1}	[202]
ZnS-Au ZnS-Ag	Hydrothermal	Methylene blue (MB) (30)	96 92	50 mg/L	ultraviolet light (6W, at 356 nm	$17.3.10^{-3}$, $18.3.10^{-3}$ min^{-1}	[203]
ZnS-Mn	Refluxing	TO (12.65)	94	500 mg/L	8 watt-UV lamp, 90 min	–	[204]
ZnS-NiS	Co-precipitation method	Methylene blue (MB) (10) RB (10)	96.91 97.12	300 mg/L	visible light 500 W tungsten halogen lamp, 150 min	0.0481 min^{-1}	[205]
ZnS-CuS	One-pot solid-phase method	Rhodamine B (RhB) (5)	97	10,000 mg/L	4 h, visible-light	0.0186 min^{-1}	[206]
ZnS-MoS_2	Chemical vapour deposition	Tetracycline (5)	81	100 mg/L	visible light 30W LED, 90 min	0.99 min^{-1}	[207]

is thermodynamically capable of reducing protons to hydrogen gas [6,9,126,219-222]. However, its efficiency is limited by visible-light inactivity and recombination losses. To address these challenges, researchers have developed ZnS-based heterostructures with narrow-bandgap semiconductors and co-catalysts that enhance charge separation [196,219-224]. ZnS based composites exhibit excellent hydrogen production rates under visible light [177,224-228].

Jiang *et al*. [177] reported that under visible light irradiation, the highest hydrogen evolution rate reached 239 μmol h^{-1} mg^{-1}, for ZnS/CdS composite and also among the best co-catalyst-free photocatalysts for hydrogen production. The average apparent quantum yield can be achieved as ~16.8% after 8 h of irradiation (monochromatic light at 420 ± 5 nm). Similarly, Gao *et al*. [226] stated the photocatalytic hydrogen evolution activity without any co-catalysts, with 50 mg of ZnS under UV-Vis light source achieving a hydrogen evolution rate of 7631.70 μmol h^{-1} g^{-1}. They described the enhancement the production of hydrogen due to generation of zinc defect under UV-Vis light, facilitate faster charge transfer and a lower recombination rate of photo-generated electron–hole pairs. Pina-Perez *et al*. [229] reported a solvothermally synthesised ZnS–ZnO composite with phase dependent photocatalytic H_2 evolution, achieving a maximum hydrogen production rate of 580 μmol h^{-1} g^{-1} at 200 ºC due to optimised ZnS-c/ZnS-h and ZnO interfacial charge transfer. The schematic band diagram for the same has been given in Fig. 14. However, He [228] showed the excellent photocatalytic activity of ZnO/ZnS/CdS three-phase composite with a rate of photocatalytic hydrogen production up to 2.64 mmol h^{-1} g^{-1}. This study highlights that the three phase co-catalyst composite photocatalyst provided a channel for rapid separation of photogenerated electrons and holes in the photocatalyst. Jayan *et al.* [214] demonstrated that a co-doped ZnS/ MoS_2 composite achieved enhanced visible-light-driven H_2 evolution of 1256 μmol h^{-1} without sacrificial agents, attributed to optimised band structure and reduced charge recombination. So, the above studies show that ZnS-based systems demonstrate promising H_2 evolution performance, though further advancements in stability, charge separation and scalable design are essential for practical applications. Table-3 summarizes the performance of ZnS based materials towards hydrogen evolution reaction as reported in literature.

Supercapacitor and battery applications: ZnS-based nanomaterials have attracted considerable attention for electrochemical energy storage applications, including both supercapacitors and rechargeable batteries, due to their tunable electronic structure and favourable redox properties [41,43,136, 239-244]. Supercapacitors, which bridge the gap between conventional capacitors and batteries, offer high power density, rapid charge–discharge rates and long cycle life [41,43]. In this context, ZnS exhibits promising pseudocapacitive behaviour arising from reversible faradaic reactions at or near the electrode surface, contributing to enhanced charge storage capacity [41,43,136,245,246]. The combination of electric double-layer capacitance and pseudocapacitance enables

TABLE-3
PHOTOCATALYTIC HYDROGEN PRODUCTION RATES FOR ZnS BASED PHOTOCATALYSTS

Photocatalyst	Method	Reaction condition	Band gap (eV)	Light source	Hydrogen evolution (H_2 gas)	Ref.
ZnO/ZnS	Hydrothermal	Na_2S/Na_2SO_3 as sacrificial agent	–	300 W Xe lamp	2.4 mmol g^{-1} h^{-1}	[230]
CdS/ZnS	Solvothermal	Na_2S and Na_2SO_3 as sacrificial reagents	–	300 W Xe lamp	239 μmol mg^{-1} h^{-1} quantum yield was ~16.8%	[177]
Co:ZnS	Solvothermal followed by bath deposition	50 mg Co:ZnS, 0.35 M Na_2S and 0.25 M Na_2SO_3 as sacrificial agent	3.31 eV (ZnS); 3.2 eV (CZS-4)	300 W Xe lamp	0.32 mmol/h, AQE = 0.41%	[133]
Eu:ZnS		Not specified	3.6 eV (ZnS); 3.39 eV (6 at% Eu:ZnS)	Simulated solar light	6 at% Eu:ZnS is 9000 μmol g^{-1} h^{-1}	[231]
NH_2-MIL-125/ZnS		10 mg photocatalyst in benzyl alcohol (1.0 mL) and acetonitrile (4.0 mL)	3.35eV	300 W Xe lamp	120 mm g^{-1} h^{-1}	[5]
ZnS/*g*-C_3N_4	Hydrothermal	Photocatalytic reforming process of glucose	–	300 W Xe lamp	229.9 μmol g^{-1} h^{-1}	[232]
ZnS-based films on Zn foils	solvothermal	80 mL of media solvent containing EDA as organic amine-ligand, BuOH	3.2-3.6 eV	254 nm Pen-Ray UV lamp	5.60 μmol h^{-1} cm^2	[227]
Fe-doped ZnS/ZnO	Ion-exchange followed by sulfurisation	0.321 g of sodium sulfide hydrate, glycerol as a sacrificial agent	3.6 eV	150 W xenon lamp	177.7 mmol m^{-2} h^{-1}	[233]
ZnO/ZnS	Co-precipitation	50 mg sample into $Na_2S{\cdot}9H_2O$ and Na_2SO_3 solution (1 mol/L)	3.49 eV	Microsolar 300 W Xenon Lamp	7.59 mmol g^{-1}	[234]
ZnS/ZnO	Solvothermal	Methanol as scarifying agent	3.4 and 3.1 eV	Solar light	580 μmol g^{-1} h^{-1}	[235]
ZnS@ZnO	Hydrothermal	0.010 g of sample and 20 mL of solution containing Na_2S (0.1 M)/Na_2SO_3 (0.2 M) as sacrificial agent	3.3 eV	300 W xenon lamp	18.81 mmol h^{-1} g^{-1}	[236]
ZnS/CdS/Zn-Cd-MOF	Semiderivatisation of bimetallic MOF strategy	10 mg catalyst, 0.25 M Na_2SO_3 and 0.35 M Na_2S	2.49 eV (CdS) 3.49 eV (ZnO) 2.27 eV (ZnS/CdS/Zn-Cd-MOF)	300 W xenon lamp	27.65 mmol g^{-1} h^{-1} AQE = 20.37%	[237]
ZnO/ZnS/Co_3O	*In situ* vulcanizing	5 mg catalyst, 10 vol% methanol	–	300 W xenon lamp	153.01 μmol g^{-1} h^{-1}	[238]

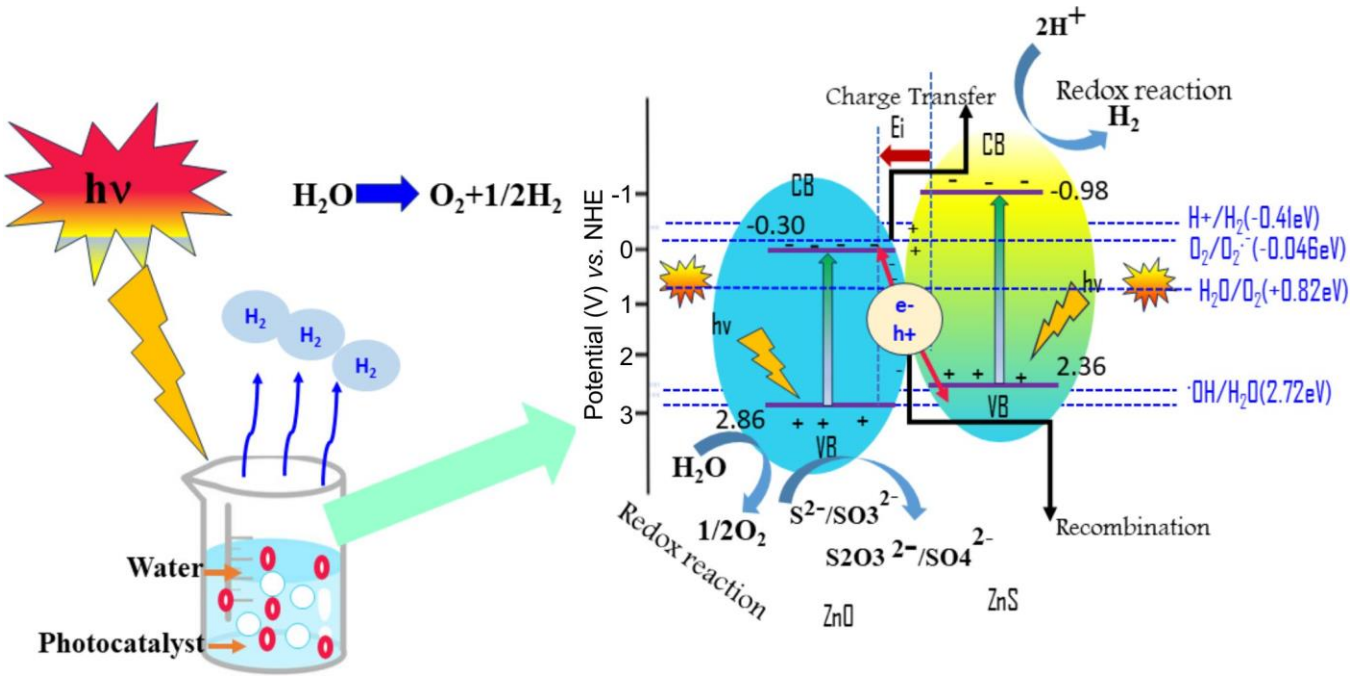

Fig. 14. Schematic diagram of H_2 production *via* photocatalytic water splitting for ZnO/ZnS composite [229]

ZnS-based materials to deliver improved electrochemical performance, particularly when engineered at the nanoscale [245,246]. Nanostructured forms such as nanoparticles, nanosheets and hierarchical architectures provide high surface area and abundant active sites, facilitating efficient ion diffusion and electron transport. In addition to supercapacitors, ZnS has also been explored as an electrode material in rechargeable battery systems, including Li^+, K^+ and Na^+ ions batteries [239-244,247-251]. However, challenges such as poor intrinsic conductivity, volume expansion and structural degradation during repeated cycling limit its practical application. To address these limitations, various strategies such as doping, defect engineering and the development of binary and ternary nanocomposites have been employed. Moreover, hybrid systems combining ZnS with metal oxides or other sulphides improve electrochemical kinetics and cycling durability through synergistic effects. Hussain *et al.* [245] reported ZnS nanoflakes grown on nickel foam exhibiting a high specific capacity of 659 C g^{-1} at 2 A g^{-1}, while the assembled asymmetric supercapacitor delivered specific capacity of 154 C g^{-1}, a high specific energy of 30 Wh kg^{-1}, high specific power of 14 kW kg^{-1} and 96% capacitance retention after 2000 cycles, demonstrating excellent electrochemical performance and stability. Arif *et al.* [248] developed a TiN–ZnS nanocomposite electrode exhibiting superior electrochemical performance, delivering an energy density of 74.13 Wh kg^{-1} and a power density of 7648 W kg^{-1} at 9 A g^{-1}, along with 96.8% capacitance retention after 10,000 cycles. A ZnS/MWCNT heterostructure anode delivered a high initial discharge capacity of 1960 mAh g^{-1} at 50 mA g^{-1}, with ~97.6% coulombic efficiency and ~94% capacity retention after 1000 cycles, highlighting strong potential for advanced Li^+ ion battery applications, as reported by Shabbir *et al.* [240]. Ti-doped ZnS thin film delivered a specific capacity of 463.1 mAh g^{-1} with good cycling stability up to 500 cycles, reflecting improved electrochemical kinetics and Li^+ diffusion upon Ti incorporation, as demonstrated by Jiang *et al.* [241]. Jin *et al.* [242] reported uniform dispersion of ZnS nanospheres on rGO which enabled enhanced electrochemical stability and Na^+ ion storage, achieving 634.6 mAh g^{-1} after 1000 cycles at 0.5 A g^{-1}. These advancements demonstrate that ZnS-based hybrid nanocomposites hold significant potential as efficient and durable materials for advanced energy storage applications.

Applications of ZnS as sensors: ZnS-based materials have been widely investigated as active sensing elements due to their semiconducting characteristics, chemical stability and strong surface adsorption behaviour [43]. ZnS is predominantly an n-type wide-band-gap semiconductor and its sensing response is governed by surface charge modulation arising from adsorption-desorption processes of gas molecules [43, 252]. Under ambient conditions, oxygen species adsorb on the ZnS surface by capturing electrons from the conduction band, leading to the formation of an electron depletion layer and an increase in electrical resistance. Exposure to reducing gases such as ammonia, hydrogen sulphide, ethanol and other volatile organic compounds results in reactions with the adsorbed oxygen species, releasing trapped electrons back into the conduction band and causing a decrease in resistance, whereas oxidizing gases enhance electron withdrawal and increase resistance [253,254]. The magnitude of the sensing response in ZnS is strongly dependent on particle size, morphology, surface defect density and crystallinity, all of which influence charge carrier concentration and surface reactivity. Nanostructured ZnS including nanoparticles, nanorods, nanowires and nanosheets, consistently exhibits improved sensing performance compared to bulk ZnS due to higher surface-to-volume ratios and a greater number of active adsorption sites [255-259]. When the crystallite size approaches the Debye length, surface adsorption events modulate the entire conduction channel, resulting in enhanced sensitivity and faster

response-recovery behaviour. The experimental studies further confirm that sulphide vacancies and other intrinsic defects act as active adsorption centres and electron donors, improving charge transfer during sensing reactions [256,257]. The controlled defect generation and elemental doping have been shown to enhance electrical conductivity and sensing response by introducing localised electronic states and facilitating carrier transport, while noble metal incorporation provides catalytic activity and promotes efficient charge exchange at the sensor surface [43,252-260]. The sensing performance of ZnS has been significantly improved through the formation of hybrid nanocomposites and heterostructured systems, which introduce interfacial electronic interactions and additional depletion regions that amplify resistance modulation [254, 259,260]. ZnS-based composites with metal oxides, layered semiconductors and carbonaceous materials exhibit enhanced charge transport, improved signal stability and reduced operating temperatures compared to pristine ZnS [259,261].

The carbon-based ZnS hybrids, in particular, provide continuous conductive pathways that facilitate rapid electron transfer and improve reproducibility over multiple sensing cycles. These engineered materials have been reliably applied for the detection of environmentally and industrially relevant gases, including ammonia and hydrogen sulphide, where ZnS shows strong and reproducible responses due to favourable surface interactions. ZnS-based sensors have also demonstrated consistent sensitivity toward volatile organic compounds such as ethanol, acetone and methanol, with selectivity governed by surface chemistry and composite design [40,259-262]. In addition to resistive gas sensing, ZnS nanostructures exhibit stable optical and photoluminescence properties that have been exploited for optical and photo-assisted sensing, where light-induced charge carriers enhance adsorption kinetics and sensing response at reduced operating temperatures. ZnS quantum dots and nanocomposites have further been employed in chemical and electrochemical sensing platforms for the detection of metal ions and small molecules, relying on experimentally validated surface interactions and charge transfer mechanisms [43,252]. Although challenges such as humidity interference, selectivity in complex environments and long-term stability remain, the sensing behaviour of ZnS and ZnS-based nanocomposites is well supported by reported experimental evidence, establishing these materials as technically reliable and multifunctional sensing platforms.

Challenges and future perspectives: Despite remarkable progress, the practical deployment of ZnS-based hybrid nanocomposites across photocatalysis, energy and sensing applications remains constrained by several fundamental and technological challenges. A key limitation originates from the intrinsic wide bandgap of ZnS, which restricts efficient solar spectrum utilisation and necessitates advanced band structure engineering. While significant progress has been achieved through doping and heterostructure formation, achieving an optimal balance between enhanced visible-light absorption and preservation of strong redox potential continues to be a critical challenge, particularly for photocatalytic applications such as pollutant degradation, hydrogen evolution and CO_2 reduction. Another major limitation arises from charge carrier dynamics, where rapid recombination of photogenerated electron–hole pairs significantly reduces quantum efficiency in photocatalytic and photoelectrochemical systems. Although several modification strategies have been developed to suppress charge recombination and enhance carrier separation, the interfacial mechanisms governing charge transfer, carrier lifetime and reaction kinetics under practical operating conditions are still not fully understood. This gap is especially critical in complex systems such as Z-scheme heterostructures and multi-component nanocomposites, where charge transfer pathways are not yet fully resolved. Photocorrosion and long-term stability represent persistent challenges for ZnS-based systems, particularly under continuous illumination and in aqueous environments. Structural degradation due to sulphide oxidation not only affects photocatalytic efficiency but also limits durability in H_2 evolution and CO_2 reduction systems. Developing intrinsically stable architectures that resist photocorrosion without relying excessively on sacrificial agents or protective coatings remains an important research direction. From an application perspective, although ZnS-based materials have shown strong potential in hydrogen evolution and CO_2 reduction, achieving high selectivity toward desired products, especially in multi-electron processes, is still challenging. In CO_2 reduction, controlling product distribution and improving C-C coupling efficiency require precise tuning of active sites and reaction intermediates. Similarly, in hydrogen evolution, reducing over potential and enhancing reaction kinetics without noble metal co-catalysts is essential for cost-effective applications. In the field of energy storage, ZnS-based materials have been extensively explored, particularly in supercapacitors and battery systems, demonstrating high theoretical capacities and promising electrochemical performance. However, challenges such as volume expansion during cycling, limited electrical conductivity and structural instability hinder their long-term performance. Moreover, translating these materials from half-cell configurations to practical full-device architectures remains a significant barrier. Bridging this gap requires the design of robust hybrid structures with improved mechanical integrity and charge transport properties. For sensing applications, ZnS-based nanocomposites offer high sensitivity and tunable surface properties; however, issues related to selectivity, response time and stability under varying environmental conditions remain unresolved. The development of highly selective sensors capable of operating under real-world conditions with minimal interference is crucial for practical deployment. Beyond individual applications, a major overarching challenge is the lack of integration of ZnS-based materials into multifunctional platforms. Although substantial progress has been achieved in individual application areas, the development of integrated systems capable of simultaneously performing photocatalysis, energy storage and sensing functions remains limited. Advancing such multifunctional platforms is crucial for the development of next-generation smart and sustainable technologies.

Looking forward, future research should focus on atomic level material design, enabling precise control over defects, interfaces and electronic structures to optimize performance across multiple applications. The integration of advanced *in situ* characterisation techniques with theoretical modelling will be critical to unravel reaction mechanisms and guide rational

material design. Furthermore, data-driven strategies and machine learning approaches provide new opportunities for accelerating the discovery and optimisation of high-performance ZnS-based materials. Parallel efforts toward scalable, cost-effective and environmentally sustainable synthesis routes are equally important for enabling industrial implementation. In addition, the development of multifunctional ZnS-based hybrid nanocomposites integrating photocatalytic, energy-storage and sensing capabilities within a single architecture represents a promising direction for future research. Such systems could enable integrated solutions for environmental remediation, renewable energy generation and real-time monitoring, thereby advancing the practical implementation of ZnS-based technologies in sustainable development.

Conclusion

This review presents a comprehensive and systematically organised assessment of recent developments in ZnS-based hybrid nanocomposites for multifunctional applications in photocatalysis, energy and sensing. It begins with an overview of ZnS fundamentals, including its crystal structure, physico-chemical properties, followed by an in-depth discussion of photocatalytic mechanisms such as charge generation, migration dynamics, band structure alignment and key enhancement strategies including doping, defect engineering and heterojunction construction. Particular emphasis is placed on photocatalytic applications, especially the degradation of organic pollutants, highlighting structure–performance relationships. Beyond photocatalysis, the review extends to energy-related applications, including CO_2 reduction and hydrogen evolution reactions, along with a detailed discussion on energy storage systems such as supercapacitors and advanced batteries, including lithium-ion, sodium-ion and potassium-ion batteries, where ZnS-based materials exhibit promising electrochemical performance. In addition, the role of ZnS-based nanocomposites in sensing applications is critically examined, focusing on their sensitivity, selectivity and multi-functional integration. Finally, the review summarises current challenges and future perspectives, highlighting the importance of rational material design, enhanced stability, scalable synthesis and the development of integrated multifunctional platforms. This work seeks to address existing research gaps by providing a unified understanding of the influence of structural and interfacial engineering on the performance and effective utilisation of ZnS-based systems across diverse technological applications.

CONFLICT OF INTEREST

The authors declare that there is no conflict of interests regarding the publication of this article.

DECLARATION OF AI-ASSISTED TECHNOLOGIES

During the preparation of this manuscript, the authors used an AI-assisted tool(s) to improve the language as well as editing of figures. The authors reviewed and edited the content and take full responsibility for the published work.

REFERENCES

1. J. Zhang, K. Qi, R. Pitcheri and C. Duan, *J. Photochem. Photobiol. Photochem. Rev.*, **65**, 100722 (2025); https://doi.org/10.1016/j.jphotochemrev.2025.100722
2. L. Isac and A. Enesca, *Int. J. Mol. Sci.*, **23**, 15668 (2022); https://doi.org/10.3390/ijms232415668
3. M. Farhan, A.K. Singh and G. Kumar, *Asian J. Chem.*, **37**, 2605 (2025); https://doi.org/10.14233/ajchem.2025.34552
4. X. Zhang, S. Xiong, A. Sathiyaseelan, L. Zhang, Y. Lu, Y. Chen, T. Jin and M.-H. Wang, *Chemosphere*, **364**, 143142 (2024); https://doi.org/10.1016/j.chemosphere.2024.143142
5. K. Zhu, Y. Yao, X. Liang, Y. Yang, H.F. Garces and K. Yan, *Green Energy Environ.*, **10**, 2327 (2025); https://doi.org/10.1016/j.gee.2025.07.006
6. A. Saravanan, P.S. Kumar, D.-V.N. Vo, P.R. Yaashikaa, S. Karishma, S. Jeevanantham, B. Gayathri and V.D. Bharathi, *Environ. Chem. Lett.*, **19**, 441 (2021); https://doi.org/10.1007/s10311-020-01077-8
7. A.S. Kumar, D.P. Pabba, N.R. Reddy and S.W. Joo, *J. Alloys Compd.*, **1031**, 180934 (2025); https://doi.org/10.1016/j.jallcom.2025.180934
8. W. Liu, W. Wang, J. Xu and S. Cao, *Surf. Interfaces*, **58**, 105846 (2025); https://doi.org/10.1016/j.surfin.2025.105846
9. M.A. Hassaan, M.A. El-Nemr, M.R. Elkatory, S. Ragab, V.-C. Niculescu and A. El Nemr, *Top. Curr. Chem. (Cham)*, **381**, 31 (2023); https://doi.org/10.1007/s41061-023-00444-7
10. S. Yadav and P. Malhotra, *Top. Catal.*, (2025); https://doi.org/10.1007/s11244-025-02200-1
11. D. Vaya and P.K. Surolia, *Environ. Technol. Innov.*, **20**, 101128 (2020); https://doi.org/10.1016/j.eti.2020.101128
12. R. Jayanthi, R. Suresh and N. Jayaprakash, *Asian J. Chem.*, **37**, 2237 (2025); https://doi.org/10.14233/ajchem.2025.34334
13. H.U. Anuforo, P.N. Abara, N.A. Chiegboka, A.C. Udebuani, O.O. Ibeh, J.C. Nnokwe, L.A. Adjeroh and T.E. Ogbulie, *Asian J. Chem.*, **37**, 2251 (2025); https://doi.org/10.14233/ajchem.2025.34247
14. V. Ponni and C. Rakkappan, *Asian J. Chem.*, **37**, 2322 (2025); https://doi.org/10.14233/ajchem.2025.34339
15. S. Vaishnavi Mahadevan and S. Raja, *Results Eng.*, **26**, 105589 (2025); https://doi.org/10.1016/j.rineng.2025.105589
16. M. Muscetta, H.S. Jarusheh, G. Williams, K.M. Alam, K. Shankar, G. Palmisano and S. Vernuccio, *Chem. Eng. J.*, **532**, 174189 (2026); https://doi.org/10.1016/j.cej.2026.174189
17. A. Vilanova, P. Dias, T. Lopes and A. Mendes, *Chem. Soc. Rev.*, **53**, 2388 (2024); https://doi.org/10.1039/D1CS01069G
18. H. Song, S. Luo, H. Huang, B. Deng and J. Ye, *ACS Energy Lett.*, **7**, 1043 (2022); https://doi.org/10.1021/acsenergylett.1c02591
19. S.A.M. Ahmed, P. Nagababu and S. Rayalu, *Discov. Electrochem.*, **2**, 68 (2025); https://doi.org/10.1007/s44373-025-00080-4
20. M.A. Darwish, W. Abd-Elaziem, A. Elsheikh and A.A. Zayed, *Nanoscale Adv.*, **6**, 4015 (2024); https://doi.org/10.1039/D4NA00214H
21. V.A. Tran, V. Vo, V.D. Doan, N.C. Thanh, N.N. Le, V.T. Le, V.H. Tran, V.M. Nguyen, H. Jeong and M.H. Tran, *ChemistrySelect*, **11**, e03508 (2026); https://doi.org/10.1002/slct.202503508
22. I. Banga, A. Paul, D.C. Poudyal, S. Muthukumar and S. Prasad, *ACS Sens.*, **8**, 3307 (2023); https://doi.org/10.1021/acssensors.3c00959
23. C.M. Costa, V.F. Cardoso, P. Martins, D.M. Correia, R. Gonçalves, P. Costa, V. Correia, C. Ribeiro, M.M. Fernandes, P.M. Martins and S. Lanceros-Méndez, *Chem. Rev.*, **123**, 11392 (2023); https://doi.org/10.1021/acs.chemrev.3c00196
24. M.-H. Lin, P.S. Parasuraman and C.-H. Ho, *ACS Omega*, **3**, 6351 (2018); https://doi.org/10.1021/acsomega.8b00260

25. M. Chandra and D. Pradhan, *ChemCatChem*, **17**, e202500395 (2025); https://doi.org/10.1002/cctc.202500395
26. H.U. Rahim, M. Qaswar, M. Wang, X. Jing and X. Cai, *J. Environ. Chem. Eng.*, **9**, 106696 (2021); https://doi.org/10.1016/j.jece.2021.106696
27. J.A. Khan, S. Ahamad, M.A.H. Ansari, M. Tauqeer, C.-H. Park, J.P. Park, C.-H. Choi and A. Mohammad, *J. Water Process Eng.*, **67**, 106151 (2024); https://doi.org/10.1016/j.jwpe.2024.106151
28. R. Mahdizadeh, P. Sangpour and H.B.M. Emrooz, *Sci. Rep.*, **15**, 30272 (2025); https://doi.org/10.1038/s41598-025-16326-5
29. S. Tiwari, S. Bishnoi and S.J. Dhoble, *J. Mol. Struct.*, **1349**, 143750 (2026); https://doi.org/10.1016/j.molstruc.2025.143750
30. A. Hernández-Gordillo, F. Tzompantzi and R. Gómez, *Int. J. Hydrogen Energy*, **37**, 17002 (2012); https://doi.org/10.1016/j.ijhydene.2012.08.097
31. Y. Meng, G. Liu, G. Zuo, X. Meng, T. Wang and J. Ye, *Nanoscale*, **14**, 14455 (2022); https://doi.org/10.1039/D2NR03703C
32. S. Kokilavani, S.A. Al-Farraj, A.M. Thomas, H.A. El-Serehy, L.L. Raju and S.S. Khan, *Ceram. Int.*, **47**, 12997 (2021); https://doi.org/10.1016/j.ceramint.2021.01.163
33. S.A. Ahmad, R. Bao, M. Arif, M. Awais, Y. Liu, H.-E. Wang and W. Zhang, *Chemistry*, **31**, e202404050 (2025); https://doi.org/10.1002/chem.202404050
34. Ü. Bayram, Ç. Özer and E. Yilmaz, *ACS Omega*, **10**, 9986 (2025); https://doi.org/10.1021/acsomega.4c07910
35. X. Hao, Y. Wang, J. Zhou, Z. Cui, Y. Wang and Z. Zou, *Appl. Catal. B*, **221**, 302 (2018); https://doi.org/10.1016/j.apcatb.2017.09.006
36. I. Vamvasakis, E.K. Andreou and G.S. Armatas, *Nanomaterials*, **13**, 2426 (2023); https://doi.org/10.3390/nano13172426
37. S. Mishra, R.K. Rajaboina and Y.-D. Jho, *ACS Appl. Energy Mater.*, **8**, 1918 (2025); https://doi.org/10.1021/acsaem.4c02827
38. A. Chakrabarti and E. Alessandri, *Appl. Nanosci.*, **5**, 116 (2024); https://doi.org/10.3390/applnano5030010
39. Z. Huang, X. Li, T. Liang, B. Ren, X. Zhang, Y. Zheng, Q. Zhang, Z. Fang, M. Wu, M. Zulfiqar, L. Jing, S. Qu, B. Chen, J. Gan and D. Peng, *Responsive Mater.*, **2**, e20240019 (2024); https://doi.org/10.1002/rpm.20240019
40. P. Kumari, S. Chattopadhyay and S. Samanta, *Discov. Appl. Sci.*, **7**, 1011 (2025); https://doi.org/10.1007/s42452-025-07672-0
41. S. Saleem, S. Khalid, M.A. Malik and A. Nazir, *Energy Fuels*, **38**, 9153 (2024); https://doi.org/10.1021/acs.energyfuels.3c04795
42. O. Ejeromedoghene, K.O. Abdulwahab, I.A. Udofia, M. Kumi and A.O. Nejo, *Energy Adv.*, **3**, 1196 (2024); https://doi.org/10.1039/D4YA00202D
43. C. Rajkumar, S. Vignesh, K. Ahmad and T.H. Oh, *Biosensors*, **15**, 730 (2025); https://doi.org/10.3390/bios15110730
44. S.K. Sharma and M.P.C. Kalita, *Next Mater.*, **6**, 100310 (2025); https://doi.org/10.1016/j.nxmate.2024.100310
45. Y.C. Goswami, R. Bisauriya, A.A. Hlaing, T.T. Moe, J.B. Kaundal, D. Aryanto and R. Yudianti, *Curr. Appl. Phys.*, **68**, 275 (2024); https://doi.org/10.1016/j.cap.2024.10.011
46. W. Zhu, *Solid State Sci.*, **118**, 106406 (2021); https://doi.org/10.1016/j.solidstatesciences.2020.106406
47. A. Raza, H. Noor and S. Riaz, *ChemistrySelect*, **10**, e05710 (2025); https://doi.org/10.1002/slct.202405710
48. S. Alhassan, A.H. Alshammari, S. Alotibi, K. Alshammari, W.S. Mohamed and N.M.A. Hadia, *Nanomaterials*, **14**, 1599 (2024); https://doi.org/10.3390/nano14191599
49. S. Maheshwari, K. Kaur, S. Bhogal and A.K. Malik, *J. Nanopart. Res.*, **27**, 189 (2025); https://doi.org/10.1007/s11051-025-06368-1
50. A. Ullah, N. Javaid, A. Rafiq, A. Samreen, S. Riaz and S. Naseem, *Results Mater.*, **24**, 100628 (2024); https://doi.org/10.1016/j.rinma.2024.100628
51. P. Mohana, R. Yuvakkumar, G. Ravi, M. Thambidurai and H.D. Nguyen, *Mater. Lett.*, **338**, 133834 (2023); https://doi.org/10.1016/j.matlet.2023.133834
52. X. Liu, Y. Zhang, S. Matsushima, T. Sugiyama, H. Hojo and H. Einaga, *ACS Appl. Energy Mater.*, **5**, 1849 (2022); https://doi.org/10.1021/acsaem.1c03323
53. M. Goswami, A. Mukherjee, A.K. Das, R. Ghosh and A.K. Meikap, *Adv. Nat. Sci.: Nanosci. Nanotechnol.*, **8**, 025018 (2017); https://doi.org/10.1088/2043-6254/aa71ec
54. H. Sonawane, J. Deore, S. Rajshri and P. Chavan, *Bionanoscience*, **13**, 879 (2023); https://doi.org/10.1007/s12668-023-01105-1
55. N. Mgedle and O.S. Oluwafemi, *J. Inorg. Organomet. Polym. Mater.*, **36**, 1425 (2026); https://doi.org/10.1007/s10904-025-03998-9
56. S. Sharmila, A. Saranya, M. Arulprakasajothi, R. Saranya, B. Srimanickam, S.K. Abel, F. Shakeel and M. Faiyazuddin, *BMC Chem.*, **18**, 204 (2024); https://doi.org/10.1186/s13065-024-01320-1
57. H. Hu, H. Liang, X. Liu, H. Jiang, M. Yi, Y. Wu, X. Hao, B. Chang and W. Zhou, *Mater. Rep.: Energy*, **5**, 100358 (2025); https://doi.org/10.1016/j.matre.2025.100358
58. S. Srivastava, S. Ranjan, L. Yadav, T. Sharma, S. Choudhary, D. Agarwal, A. Singh, S. Satapathi, R.K. Gupta, A. Garg and K.S. Nalwa, *Commun. Mater.*, **4**, 52 (2023); https://doi.org/10.1038/s43246-023-00379-y
59. E.H. Khader, S.A. Muslim, N.M.C. Saady, N.S. Ali, I.K. Salih, T.J. Mohammed, T.M. Albayati and S. Zendehboudi, *Desalination Water Treat.*, **318**, 100384 (2024); https://doi.org/10.1016/j.dwt.2024.100384
60. N. Ojha, K.K. Pant and E. Coy, *Ind. Eng. Chem. Res.*, **62**, 21885 (2023); https://doi.org/10.1021/acs.iecr.3c03426
61. S.M. Yahaya, N. Abdu, I.A. Aliyu and B. Mukhtar, *Circ. Agric. Syst.*, **4**, e015 (2024); https://doi.org/10.48130/cas-0024-0014
62. S. Kalantari and A. Shokuhfar, *Sci. Rep.*, **14**, 11669 (2024); https://doi.org/10.1038/s41598-024-62611-0
63. T.-F. Yi, Y. Li, Y.-M. Li, S. Luo and Y.-G. Liu, *Solid State Ion.*, **343**, 115074 (2019); https://doi.org/10.1016/j.ssi.2019.115074
64. H.U. Rehman, H. Khan, Z. Abbasi, L. Ben Tahar, R.A. Khan, A. Waseem and A.J. Shaikh, *Mater. Adv.*, **6**, 7847 (2025); https://doi.org/10.1039/D5MA00846H
65. J. Cui, D. Ding, S. Yue and Z.D. Chen, *ACS Appl. Energy Mater.*, **8**, 14093 (2025); https://doi.org/10.1021/acsaem.5c01370
66. F. Kurnia, Y.H. Ng, Y. Tang, R. Amal, N. Valanoor and J.N. Hart, *Cryst. Growth Des.*, **16**, 2461 (2016); https://doi.org/10.1021/acs.cgd.5b01590
67. N.N. Rosman, N.R.A.M. Shah, N.F.M. Siti, K. Arifin, L.J. Minggu, N.A. Ludin and R.M. Yunus, *Int. J. Hydrogen Energy*, **104**, 324 (2025); https://doi.org/10.1016/j.ijhydene.2024.06.204
68. Q.Y. Wang, Z.F. Wu, M. Zhang, Z.J. Qin, L. Wang, F.R. Zhong and H.M. Duan, *J. Electron. Mater.*, **51**, 3843 (2022); https://doi.org/10.1007/s11664-022-09644-1
69. J. Guo, C. Wang, X. Chang, W. Zheng, J. Zhang and X. Liu, *ACS Appl. Electron. Mater.*, **7**, 3552 (2025); https://doi.org/10.1021/acsaelm.5c00285
70. H. Dehghani, S. Khoramnejadian, M. Mahboubi, M. Sasani, S. Ghobadzadeh, S.M. Haghighi and M. Negahdary, *Int. J. Electrochem. Sci.*, **11**, 2029 (2016); https://doi.org/10.1016/S1452-3981(23)16080-9
71. N.R. Barveen, S. Chinnapaiyan, C.-H. Huang, Y.-Y. Lin, J.-L. Xu and Y.-W. Cheng, *Anal. Chim. Acta*, **1328**, 343177 (2024); https://doi.org/10.1016/j.aca.2024.343177
72. S. Wang, H. Li, X. Wan, B. Jiang, C. Yao, J. Liu and Y. Yang, *Surf. Interfaces*, **71**, 106883 (2025); https://doi.org/10.1016/j.surfin.2025.106883
73. M.Y.A. Rahman, S.N. Sadikin and A.A. Umar, *Int. J. Electrochem. Sci.*, **17**, 22049 (2022); https://doi.org/10.20964/2022.04.24

74. D. Diaz-Diestra, H.M. Gholipour, M. Bazian, B. Thapa and J. Beltran-Huarac, *Nanoscale Res. Lett.*, **17**, 33 (2022); https://doi.org/10.1186/s11671-022-03674-8
75. A. Shamirian, O. Appelbe, Q. Zhang, B. Ganesh, S.J. Kron and P.T. Snee, *J. Mater. Chem. B*, **3**, 8188 (2015); https://doi.org/10.1039/C5TB00247H
76. Y. Zhang, M. Zhang, Z. Yu, R. Liu, Y. Li, J. Xiong, Y. Qiao, R. Zhang and X. Lu, *Appl. Catal. B*, **350**, 123914 (2024); https://doi.org/10.1016/j.apcatb.2024.123914
77. F. Kang, C. Xu, C. Wang, Z. Huang, H. Ma, C. Chen and J. Hu, *Green Chem.*, **28**, 5788 (2026); https://doi.org/10.1039/D5GC06931A
78. C.S. Ho and M.-H. Lin, *RSC Adv.*, **6**, 81053 (2016); https://doi.org/10.1039/C6RA15150G
79. S. Liu, F. Fan, P. Li, R. Sun, Y. Wan, K. Chang and Y. Zhou, *J. Phys. Chem. Lett.*, **14**, 9978 (2023); https://doi.org/10.1021/acs.jpclett.3c02675
80. H. Pang, X. Meng, P. Li, K. Chang, W. Zhou, X. Wang, X. Zhang, W. Jevasuwan, N. Fukata, D. Wang and J. Ye, *ACS Energy Lett.*, **4**, 1387 (2019); https://doi.org/10.1021/acsenergylett.9b00711
81. S. Shen, C. Yuan, Y. Xu, Y. Xie, L. Wang, T. Yan, S. Chen, L. Wang, T. Liu and L. Zhang, *Adv. Funct. Mater.*, **35**, 2420258 (2025); https://doi.org/10.1002/adfm.202420258
82. H. Hao, L. Zhang, W. Wang, S. Qiao and X. Liu, *ACS Sustain. Chem.& Eng.*, **7**, 10501 (2019); https://doi.org/10.1021/acssuschemeng.9b01017
83. D. Moher, A. Liberati, J. Tetzlaff and D.G. Altman, *J. Clin. Epidemiol.*, **62**, 1006 (2009); https://doi.org/10.1016/j.jclinepi.2009.06.005
84. N.R. Haddaway, M.J. Page, C.C. Pritchard and L.A. McGuinness, *Campbell Syst. Rev.*, **18**, e1230 (2022); https://doi.org/10.1002/cl2.1230
85. D. Moore and Z.L. Wang, *J. Mater. Chem.*, **16**, 3898 (2006); https://doi.org/10.1039/b607902b
86. J.L. Fenton, B.C. Steimle and R.E. Schaak, *Inorg. Chem.*, **58**, 672 (2019); https://doi.org/10.1021/acs.inorgchem.8b02880
87. T. Lange, S. Reichenberger, S. Ristig, M. Rohe, J. Strunk, S. Barcikowski and R. Schlögl, *Prog. Mater. Sci.*, **124**, 100865 (2022); https://doi.org/10.1016/j.pmatsci.2021.100865
88. Sunaina, S. Devi, S.T. Nishanthi, S.K. Mehta, A.K. Ganguli and M. Jha, *SN Appl. Sci.*, **3**, 689 (2021); https://doi.org/10.1007/s42452-021-04643-z
89. V. Nedelkovski, M. Radovanović and M. Antonijević, *ChemEngineering*, **9**, 120 (2025); https://doi.org/10.3390/chemengineering9060120
90. J. Mohammed, E.R. Elsharkawy, S.M. El-Bahy, H.Y. Hafeez, R.I. Musa, S.A. Idris, S. Maikudi and Z.M. El-Bahy, *Mater. Today Sustain.*, **32**, 101227 (2025); https://doi.org/10.1016/j.mtsust.2025.101227
91. R. Ghamarpoor, A. Fallah and M. Jamshidi, *ACS Omega*, **9**, 25457 (2024); https://doi.org/10.1021/acsomega.3c08717
92. G.-J. Lee and J.J. Wu, *Powder Technol.*, **318**, 8 (2017); https://doi.org/10.1016/j.powtec.2017.05.022
93. S. Wang, X. Niu, L. Wang, J. Bi, W. Yang and H. Hou, *Microstructures*, **5**, 2025074 (2025); https://doi.org/10.20517/microstructures.2024.116
94. D. Sahu and N.R. Panda, *Chemosphere*, **350**, 141014 (2024); https://doi.org/10.1016/j.chemosphere.2023.141014
95. S.K. Sahu and D. Sahu, *Results Opt.*, **18**, 100787 (2025); https://doi.org/10.1016/j.rio.2025.100787
96. A. Meher, N.R. Panda, S. Jal and D. Sahu, *Surf. Interfaces*, **72**, 107225 (2025); https://doi.org/10.1016/j.surfin.2025.107225
97. N.R. Panda, S.P. Pati and D. Sahu, *Next Mater.*, **10**, 101362 (2026); https://doi.org/10.1016/j.nxmate.2025.101362
98. A. Meher, N.R. Panda and D. Sahu, *Inorg. Chem. Commun.*, **180**, 115106 (2025); https://doi.org/10.1016/j.inoche.2025.115106
99. A. Palai, N.R. Panda and D. Sahu, *ECS J. Solid State Sci. Technol.*, **12**, 076015 (2023); https://doi.org/10.1149/2162-8777/ace84c
100. T.N. Krishna, B.V. Tirupanyam and M.S. Laxmi, *J. Mater. Sci.*, **60**, 19755 (2025); https://doi.org/10.1007/s10853-025-11612-z
101. L. Liu, L. Wang, D. Sun, X. Sun, L. Liu, W. Zhao, R. Tayebee and B. Liu, *ACS Omega*, **8**, 44276 (2023); https://doi.org/10.1021/acsomega.3c06952
102. P.K. Mishra, N.R. Panda, T. Yadav, S.K. Biswal and D. Sahu, *J. Mater. Sci. Mater. Electron.*, **34**, 2068 (2023); https://doi.org/10.1007/s10854-023-11526-z
103. D. Sahu and N.R. Panda, *Curr. Nanosci.*, **17**, 162 (2021); https://doi.org/10.2174/1573413716999200728175722
104. A. Meher, A. Palai, N.R. Panda and D. Sahu, *Environ. Sci. Pollut. Res. Int.*, **32**, 22121 (2025); https://doi.org/10.1007/s11356-024-35804-3
105. A. Palai, N.R. Panda, S. Chhotaray and D. Sahu, *Surf. Interfaces*, **41**, 103217 (2023); https://doi.org/10.1016/j.surfin.2023.103217
106. N.R. Panda, S.K. Sahu, A. Palai, T. Yadav, D. Behera and D. Sahu, *Chem. Phys. Impact*, **8**, 100550 (2024); https://doi.org/10.1016/j.chphi.2024.100550
107. P.K. Mishra, N.R. Panda, S.P. Pati, S.K. Biswal and D. Sahu, *ECS J. Solid State Sci. Technol.*, **10**, 071006 (2021); https://doi.org/10.1149/2162-8777/ac0cc6
108. A. Palai, N.R. Panda, M.R. Sahoo and D. Sahu, *J. Mater. Sci. Mater. Electron.*, **33**, 9599 (2022); https://doi.org/10.1007/s10854-021-07583-x
109. D. Dash, N.R. Panda and D. Sahu, *Nano Express*, **2**, 010007 (2021); https://doi.org/10.1088/2632-959X/abd90b
110. A. Palai, N.R. Panda and D. Sahu, *J. Mol. Struct.*, **1244**, 131245 (2021); https://doi.org/10.1016/j.molstruc.2021.131245
111. Y. Zhigalenok, A. Tazhibayeva, S. Kokhmetova, A. Starodubtseva, T. Kana and F. Malchik, *RSC Adv.*, **15**, 40581 (2025); https://doi.org/10.1039/D5RA06395G
112. S.K. Sahoo, L. Acharya, L. Biswal, P. Priyadarshini and K. Parida, *Inorg. Chem. Front.*, **11**, 4914 (2024); https://doi.org/10.1039/D4QI00950A
113. A. Fattah-alhosseini, Z. Sangarimotlagh and M. Karbasi, *Int. J. Hydrogen Energy*, **79**, 771 (2024); https://doi.org/10.1016/j.ijhydene.2024.07.058
114. L. El Gaini, *Desalination Water Treat.*, **320**, 100798 (2024); https://doi.org/10.1016/j.dwt.2024.100798
115. P. Pavel, C. Anastasescu, R.-N. State, A. Vasile, F. Papa and I. Balint, *Catalysts*, **13**, 380 (2023); https://doi.org/10.3390/catal13020380
116. Y. Zhang, N. Zhang, Z.-R. Tang and Y.-J. Xu, *ACS Nano*, **6**, 9777 (2012); https://doi.org/10.1021/nn304154s
117. J. Kou, C. Lu, J. Wang, Y. Chen, Z. Xu and R.S. Varma, *Chem. Rev.*, **117**, 1445 (2017); https://doi.org/10.1021/acs.chemrev.6b00396
118. B. Singh and A. Draksharapu, *Mater. Chem. Front.*, **9**, 2287 (2025); https://doi.org/10.1039/D5QM00354G
119. X. Liu, X. Li, L. Zhang, C. Ma, Y. Chen, X. Wang, H. Wei and P. Wang, *Polymers*, **17**, 575 (2025); https://doi.org/10.3390/polym17050575
120. C.V. Reddy, M. Vijayalakshmi, N. Bandaru, B. Cheolho and J. Shim, *J. Alloys Compd.*, **1043**, 184244 (2025); https://doi.org/10.1016/j.jallcom.2025.184244
121. M.E. Khan, *Catalysts*, **14**, 888 (2024); https://doi.org/10.3390/catal14120888
122. T. Bekele and G. Alamnie, *Results Chem.*, **18**, 102758 (2025); https://doi.org/10.1016/j.rechem.2025.102758
123. S. Wang, F. Gao, X. Niu, L. Wang, Y. Yang, D. Yang, W. Yang and H. Hou, *Appl. Catal. B*, **382**, 125931 (2026); https://doi.org/10.1016/j.apcatb.2025.125931
124. L.A. Ramos-Huerta, O. Aguilar-Martínez, V. Santes, F.J. Tzompantzi Morales and C.E. Santolalla-Vargas, *Chem. Eng. Sci.*, **294**, 120067 (2024); https://doi.org/10.1016/j.ces.2024.120067
125. K. Mróz, M. Kobielusz, Ł. Orzeł and W. Macyk, *J. Phys. Chem. C Nanomater. Interfaces*, **127**, 17366 (2023); https://doi.org/10.1021/acs.jpcc.3c04298
126. E. Kang and J.H. Kim, *J. Environ. Chem. Eng.*, **11**, 109833 (2023); https://doi.org/10.1016/j.jece.2023.109833
127. S.P. Sarangi, S. Mishra and N. Behera, *Mater. Sci. Semicond. Process.*, **147**, 106723 (2022); https://doi.org/10.1016/j.mssp.2022.106723

128. H.M. Mistry, M.P. Deshpande, A.B. Hirpara, N.M. Suchak, S.H. Chaki and S.V. Bhatt, *Opt. Mater.*, **159**, 116529 (2025); https://doi.org/10.1016/j.optmat.2024.116529
129. H. Li, C. Li, H. Huang, G. Hao and F. Wang, *Int. J. Mod. Phys. B*, **38**, 2450365 (2024); https://doi.org/10.1142/S021797922450365X
130. P. Devaraji, M. Mapa, H.M.A. Hakkeem, K. Krishnamoorthy, V. Sudhakar, and C.S. Gopinath, *ACS Omega*, **2**, 6768 (2017); https://doi.org/10.1021/acsomega.7b01172
131. C.M. Lee, P. Palaniandy and I. Dahlan, *Environ. Earth Sci.*, **76**, 611 (2017); https://doi.org/10.1007/s12665-017-6924-y
132. S.J. Xie, Q.H. Zhang, G.D. Liu and Y. Wang, *Chem. Commun.*, **52**, 35 (2016); https://doi.org/10.1039/C5CC07613G
133. B. Poornaprakash, U. Chalapathi, M. Kumar, S.V.P. Vattikuti, B. Rajitha, P.T. Poojitha and S.-H. Park, *Mater. Sci. Semicond. Process.*, **121**, 105395 (2021); https://doi.org/10.1016/j.mssp.2020.105395
134. S.K. Sahu, N.R. Panda and D. Sahu, *J. Cluster Sci.*, **37**, 37 (2026); https://doi.org/10.1007/s10876-026-02993-5
135. V.C. Jasna, T. Anilkumar and M.T. Ramesan, *J. Appl. Polym. Sci.*, **135**, 46538 (2018); https://doi.org/10.1002/app.46538
136. M.S. Shah, Z. Zhenyu, S. Ahmad, S. Wang, H. Hou, X. Zuo and M.Z.U. Shah, *Surf. Interfaces*, **75**, 107750 (2025); https://doi.org/10.1016/j.surfin.2025.107750
137. H. Salaheldin, A. Aboelnga and A. Elsayed, *Sci. Rep.*, **14**, 32165 (2024); https://doi.org/10.1038/s41598-024-81855-4
138. B.A. Bhat, N. Jadon, L. Dubey and S.A. Mir, *ACS Omega*, **9**, 24425 (2024); https://doi.org/10.1021/acsomega.4c00247
139. H.M. Hussein, *Colloid J.*, **85**, 666 (2023); https://doi.org/10.1134/S1061933X22600610
140. R. Qin, Y. Zhou, Y. Huang, Y. Zhao and L. Hao, *Inorg. Nano-Met. Chem.*, **55**, 599 (2025); https://doi.org/10.1080/24701556.2024.2353764
141. G. Saavedra-Rodriguez, U. Pal, R. Sánchez-Zeferino and M.E. Álvarez-Ramos, *J. Phys. Chem. C Nanomater. Interfaces*, **124**, 3857 (2020); https://doi.org/10.1021/acs.jpcc.9b10890
142. W.S. Mohamed, M. Ezzeldien, A.H. Alshammari, K. Alshammari, S. Alhassan and N.M.A. Hadia, *Opt. Mater.*, **157**, 116345 (2024); https://doi.org/10.1016/j.optmat.2024.116345
143. A. Hussain, M. Ahmad, X. Chen, N. Abbas, S. Al Arni, A.M. Salih, M. Benaissa, M. Ashraf, M. Ayaz, M. Imran, M.Z. Ansari and K. Zhang, *J. Saudi Chem. Soc.*, **26**, 101510 (2022); https://doi.org/10.1016/j.jscs.2022.101510
144. A. Shaukat, F. Shaheen, K.S. Munawar, S. Mehmood, R. Fatima, S. Yousuf and M. Imran, *J. Mol. Struct.*, **1335**, 141957 (2025); https://doi.org/10.1016/j.molstruc.2025.141957
145. H.V. Bui, D.V. Thai, T.D. Nguyen, V.N. Lam, H.T. Tran, V.M. Nguyen, N.D. Nui and N.M. Hung, *Mater. Chem. Phys.*, **307**, 128081 (2023); https://doi.org/10.1016/j.matchemphys.2023.128081
146. L.B. Chandrasekar, R. Chandramohan, R. Vijayalakshmi and S. Chandrasekaran, *Int. Nano Lett.*, **5**, 71 (2015); https://doi.org/10.1007/s40089-015-0139-6
147. D.M. Sousa, L.C. Alves, A. Marques, G. Gaspar, J.C. Lima and I. Ferreira, *Sci. Rep.*, **8**, 15992 (2018); https://doi.org/10.1038/s41598-018-34268-z
148. L. Dai, C. Strelow, T. Kipp, A. Mews, I. Benkenstein, D. Eifler, T.H. Vuong, J. Rabeah, J. McGettrick, R. Lesyuk and C. Klinke, *Chem. Mater.*, **33**, 275 (2021); https://doi.org/10.1021/acs.chemmater.0c03755
149. S.K. Sahu, N.R. Panda and D. Sahu, *J. Indian Chem. Soc.*, **102**, 102309 (2025); https://doi.org/10.1016/j.jics.2025.102309
150. A. Pole and P. Borker, *Micro Nano Struct.*, **211**, 208546 (2026); https://doi.org/10.1016/j.micrna.2025.208546
151. L. Bibi, T. Iqbal, M. Seemab, S. Afsheen, I.M. Ashraf, F. Saeed, A.M. Ali, M. Yousaf and M.A. Sayed, *J. Environ. Chem. Eng.*, **14**, 120933 (2026); https://doi.org/10.1016/j.jece.2025.120933
152. Y. Li, X. Zhang, J. Zheng, T. Xiao, Q. Fu, C. Yang, D. Wang and G. Zhang, *Chem. Eng. J.*, **497**, 154816 (2024); https://doi.org/10.1016/j.cej.2024.154816
153. H. Sudrajat and M. Nobatova, *RSC Appl. Interfaces*, **2**, 599 (2025); https://doi.org/10.1039/D5LF00037H
154. P. Yadav, A.C. Asokan, J. Yadav and B.S. Naidu, *ACS Appl. Energy Mater.*, **8**, 16739 (2025); https://doi.org/10.1021/acsaem.5c02585
155. D. Salazar-Marín, G. Oza, J.A. Díaz Real, A. Cervantes-Uribe, H. Pérez-Vidal, M.K. Kesarla, J.G. Torres Torres and S. Godavarthi, *Appl. Surf. Sci. Adv.*, **19**, 100536 (2024); https://doi.org/10.1016/j.apsadv.2023.100536
156. K.K. Mandari and M. Kang, *Adv. Ind. Eng. Chem.*, **1**, 14 (2025); https://doi.org/10.1007/s44405-025-00014-z
157. I.S. Popov, N.S. Kozhevnikova, M.A. Melkozerova, A.S. Vorokh and A.N. Enyashin, *Mater. Chem. Phys.*, **215**, 176 (2018); https://doi.org/10.1016/j.matchemphys.2018.04.115
158. D. Kanakaraju and A. Chandrasekaran, *Sci. Total Environ.*, **868**, 161525 (2023); https://doi.org/10.1016/j.scitotenv.2023.161525
159. X. Dong, F. Zhang, C. Rong and H. Ma, *Scient. World J.*, **2014**, 503895 (2014); https://doi.org/10.1155/2014/503895
160. S. Talebi, N. Chaibakhsh and Z. Moradi-Shoeili, *J. Appl. Res. Technol.*, **15**, 378 (2017); https://doi.org/10.1016/j.jart.2017.03.007
161. A.M. Laera, L. Mirenghi, G. Cassano, L. Capodieci, M.C. Ferrara, S. Mazzarelli, M. Schioppa, D. Dimaio, A. Rizzo, M. Penza and L. Tapfer, *Thin Solid Films*, **709**, 138190 (2020); https://doi.org/10.1016/j.tsf.2020.138190
162. Y.-H. Nien, J.-W. Zeng, Y.-H. Huang, J.-C. Chou, C.-H. Lai, P.-Y. Kuo, P.-H. Yang, Y.-W. Chen and W.-H. Chen, *IEEE Trans. Semicond. Manuf.*, **38**, 332 (2025); https://doi.org/10.1109/TSM.2025.3550570
163. S. Khan, M. Je, N.N.T. Ton, W. Lei, T. Taniike, S. Yanagida, D. Ogawa, N. Suzuki, C. Terashima, A. Fujishima, H. Choi and K. Katsumata, *Appl. Catal. B*, **297**, 120473 (2021); https://doi.org/10.1016/j.apcatb.2021.120473
164. S. Shreya, P. Phogat, R. Jha and S. Singh, *ECS Meet. Abstr.*, **MA2024-01**, 2894 (2024); https://doi.org/10.1149/MA2024-01542894mtgabs
165. S. Khosravi, N. Chaibakhsh, S. Jafari and M. Nilkar, *Sci. Rep.*, **14**, 28385 (2024); https://doi.org/10.1038/s41598-024-78009-x
166. F. Shi, L. Chen, C. Xing, D. Jiang, D. Li and M. Chen, *RSC Adv.*, **4**, 62223 (2014); https://doi.org/10.1039/C4RA11740A
167. G.M. Manoj, H. Shankar and V.K. Ponnusamy, *Diamond Rel. Mater.*, **162**, 113241 (2026); https://doi.org/10.1016/j.diamond.2025.113241
168. G. Ramalingam, P. Arunkumar, M.D. Alqahtani and A.M. Elgarahy, *Water Air Soil Pollut.*, **236**, 481 (2025); https://doi.org/10.1007/s11270-025-08082-z
169. S. Tian, H. Ren, Z. Liu, Z. Miao, L. Tian, J. Li, Y. Liu, S. Wei and P. Wang, *Catal. Commun.*, **164**, 106422 (2022); https://doi.org/10.1016/j.catcom.2022.106422
170. L. Schumacher and R. Marschall, *Top. Curr. Chem.*, **380**, 53 (2022); https://doi.org/10.1007/s41061-022-00406-5
171. S. Wang, W. Hao, Z. Liu, X. Niu, L. Wang and Q. Zhao, *ACS Nano*, **20**, 137 (2026); https://doi.org/10.1021/acsnano.5c18705
172. Q. Xu, L. Zhang, J. Yu, S. Wageh, A.A. Al-Ghamdi and M. Jaroniec, *Mater. Today*, **21**, 1042 (2018); https://doi.org/10.1016/j.mattod.2018.04.008
173. J. Li, H. Yuan, W. Zhang, B. Jin, Q. Feng, J. Huang and Z. Jiao, *Carbon Energy*, **4**, 294 (2022); https://doi.org/10.1002/cey2.179
174. J. Zhang, J. Wei, J. Li, M. Xiahou, Z. Sun, A. Cao, Y. Yuanfeng, G. Chen and Y. Chen, *ACS Appl. Nano Mater.*, **7**, 20101 (2024); https://doi.org/10.1021/acsanm.4c02744
175. M. Khodamorady and K. Bahrami, *Sci. Rep.*, **13**, 2177 (2023); https://doi.org/10.1038/s41598-023-28725-7
176. J. Madhavi and V. Prasad, *Surf. Interfaces*, **21**, 100757 (2020); https://doi.org/10.1016/j.surfin.2020.100757
177. D. Jiang, Z. Sun, H. Jia, D. Lu and P. Du, *J. Mater. Chem. A Mater. Energy Sustain.*, **4**, 675 (2016); https://doi.org/10.1039/C5TA07420G

178. J. Rashid, S. Mushtaq, F. Imtiaz and M. Xu, *Mater. Sci. Semicond. Process.*, **174**, 108236 (2024); https://doi.org/10.1016/j.mssp.2024.108236
179. J. Behin, P. Amiri and S. Ghabaee, *J. Environ. Manage.*, **389**, 126166 (2025); https://doi.org/10.1016/j.jenvman.2025.126166
180. J. Dong, W. Fang, H. Yuan, W. Xia, X. Zeng and W. Shangguan, *ACS Appl. Energy Mater.*, **5**, 4893 (2022); https://doi.org/10.1021/acsaem.2c00301
181. B. Liu, X. Hu, X. Li, Y. Li, C. Chen and K. Lam, *Sci. Rep.*, **7**, 16396 (2017); https://doi.org/10.1038/s41598-017-16732-4
182. Y. Qin, W. Zhao, Z. Sun, X. Liu, G. Shi, Z. Liu, D. Ni and Z. Ma, *Adsorpt. Sci. Technol.*, **37**, 764 (2019); https://doi.org/10.1177/0263617418810932
183. L. Bao, X. Ren, C. Liu, X. Liu, C. Dai, Y. Yang, M. Bououdina, S. Ali and C. Zeng, *Chem. Commun.*, **59**, 11280 (2023); https://doi.org/10.1039/D3CC03436D
184. S. Vignesh and H. Kim, *J. Alloys Compd.*, **942**, 169077 (2023); https://doi.org/10.1016/j.jallcom.2023.169077
185. M. Hosseini-Sarvari and H. Sheikh, *React. Chem. Eng.*, **7**, 2202 (2022); https://doi.org/10.1039/D2RE00194B
186. X. Chen and H. Zhang, *Opt. Mater.*, **141**, 113968 (2023); https://doi.org/10.1016/j.optmat.2023.113968
187. W. Yang, W. Wang, S. Huang, M. Gao, F. Weng and R. Zou, *Dalton Trans.*, **54**, 4039 (2025); https://doi.org/10.1039/D4DT03381G
188. A. Alnoaimi, N. Tamimi, I.O. Alade, A. Manda, B. Sultan, S. Akhtar, M. Fatty, K.A. Elsayed and Q.A. Drmosh, *Mater. Res. Express*, **10**, 125007 (2023); https://doi.org/10.1088/2053-1591/ad1314
189. P. Wei, X. Yu and Y. Li, *J. Electron. Mater.*, **48**, 4877 (2019); https://doi.org/10.1007/s11664-019-07270-y
190. N. Mintcheva, G. Gicheva, M. Panayotova, W. Wunderlich, A.A. Kuchmizhak and S.A. Kulinich, *Materials*, **12**, 3313 (2019); https://doi.org/10.3390/ma12203313
191. Q. Ma, Y. Wang, J. Kong and H. Jia, *Ceram. Int.*, **42**, 2854 (2016); https://doi.org/10.1016/j.ceramint.2015.11.021
192. V. Vaiano, O. Sacco, D. Barba and V. Palma, *Chem. Eng. Trans.*, **74**, 1159 (2019); https://doi.org/10.3303/CET1974194
193. M.K. Aulakh, J. Dua and B. Pal, *Sep. Purif. Technol.*, **281**, 119869 (2022); https://doi.org/10.1016/j.seppur.2021.119869
194. X. Zhang, C. Shan, S. Ma, S. Zhao and J. Yang, *Inorg. Chem. Commun.*, **135**, 109089 (2022); https://doi.org/10.1016/j.inoche.2021.109089
195. A. Phuruangrat, K. Karthik, B. Kuntalue, P. Dumrongrojthanath, S. Thongtem and T. Thongtem, *Chalcogenide Lett.*, **16**, 387 (2019).
196. J. You, C. Liu, X. Feng, B. Lu, L. Xia and X. Zhuang, *Carbohydr. Polym.*, **288**, 119332 (2022); https://doi.org/10.1016/j.carbpol.2022.119332
197. M. Riazian and M. Yousefpoor, *Int. J. Smart Nano Mater.*, **11**, 47 (2020); https://doi.org/10.1080/19475411.2019.1710001.
198. Z. Ye, L. Kong, F. Chen, Z. Chen, Y. Lin and C. Liu, *Optik*, **164**, 345 (2018); https://doi.org/10.1016/j.ijleo.2018.03.030.
199. A. Dumbrava, D. Berger, G. Prodan, C. Matei, F. Moscalu and A. Diacon, *Mater. Chem. Phys.*, **193**, 316 (2017); https://doi.org/10.1016/j.matchemphys.2017.02.040
200. S.A. Thomas, S.A. Kadam, Y.-R. Ma and A. Aravind, *ChemistrySelect*, **6**, 10015 (2021); https://doi.org/10.1002/slct.202102109
201. H. Yu, H. Fang, F. Qiu, F. Meng, H. Liu, S. Wang, P. Lv, X. Cong, Q. Niu and T. Li, *Nanomaterials*, **11**, 1451 (2021); https://doi.org/10.3390/nano11061451
202. T. Amuthan, R. Sanjeevi, G.R. Kannan and A. Sridevi, *Physica B*, **638**, 413842 (2022); https://doi.org/10.1016/j.physb.2022.413842
203. M. Madkour and F. Al Sagheer, *Opt. Mater. Express*, **7**, 158 (2017); https://doi.org/10.1364/OME.7.000158
204. J. Luciano-Velázquez, Y. Xin, Y. Su, C.I. Quiles-Vélez, S.A. Cruz-Romero, G.E. Torres-Mejías, J. Rivera-De Jesús and S.J. Bailón-Ruiz, *MRS Adv.*, **6**, 252 (2021); https://doi.org/10.1557/s43580-021-00035-y
205. V. Alagarsamy, N. Venkatesh, S. Pandurengan, L. Gnanasekaran, S.A. Roshan, K. Viswanathan and G. Murugadoss, *Chem. Phys. Impact*, **11**, 100912 (2025); https://doi.org/10.1016/j.chphi.2025.100912
206. R. Mugumo, E. Ichipi, S.M. Tichapondwa and E.M.N. Chirwa, *Catalysts*, **13**, 1184 (2023); https://doi.org/10.3390/catal13081184.
207. Z. Amiri, H.B. Motejadded Emrooz and M. Safarzadeh Khosrowshahi, *Sci. Rep.*, **15**, 22086 (2025); https://doi.org/10.1038/s41598-025-08920-4
208. Y. Li, Y. Wei, J. Xiong, Z. Tang, Y. Wang, X. Wang, Z. Zhao and J. Liu, *Chem. Eng. Sci.*, **292**, 120017 (2024); https://doi.org/10.1016/j.ces.2024.120017
209. Ž. Kovačič, B. Likozar and M. Huš, *ACS Catal.*, **10**, 14984 (2020); https://doi.org/10.1021/acscatal.0c02557
210. B. Pathak, N. Sarma, K.C. Handique, H. Das, P. Saikia and P.K. Kalita, *Emergent Mater.*, **8**, 5387 (2025); https://doi.org/10.1007/s42247-025-01283-6
211. D. Masekela, P.J. Mafa, T.L. Yusuf, S.A. Balogun, A.T. Kuvarega and K.D. Modibane, *Coord. Chem. Rev.*, **549**, 217270 (2026); https://doi.org/10.1016/j.ccr.2025.217270
212. H.-i Nam, K. Ryeol Park, Y.-W. Choi, H. Sim, K. Yong Sohn and D.-H. Lim, *Appl. Surf. Sci.*, **612**, 155646 (2023); https://doi.org/10.1016/j.apsusc.2022.155646
213. W. Luo, A. Li, B. Yang, H. Pang, J. Fu, G. Chen, M. Liu, X. Liu, R. Ma, J. Ye and N. Zhang, *ACS Appl. Mater. Interfaces*, **15**, 15387 (2023); https://doi.org/10.1021/acsami.2c21966
214. G. Jayan, L. Elias, A. Anil, T.C. Bhagya and S.M.A. Shibli, *Int. J. Hydrogen Energy*, **51**, 1375 (2024); https://doi.org/10.1016/j.ijhydene.2023.11.102
215. Y. Guo, X. Tan, T. Yu and J. Gong, *Adv. Funct. Mater.*, **36**, e22276 (2026); https://doi.org/10.1002/adfm.202522276
216. H. Fu, Y. Wu, Y. Guo, T. Sakurai, Q. Zhang, Y. Liu, Z. Zheng, H. Cheng, Z. Wang, B. Huang, Q. Wang, K. Domen and P. Wang, *Nat. Commun.*, **16**, 990 (2025); https://doi.org/10.1038/s41467-025-56314-x
217. Y. Mohammed, H.Y. Hafeez, K.M. Al-Ahmary, J.S. Alnawmasi, Z. Alqahtani, S.R. Al-Mhyawi, S.B. Alotaibi, J. Mohammed and C.E.R. Ndikilar, *Mater. Chem. Phys.*, **348**, 131551 (2026); https://doi.org/10.1016/j.matchemphys.2025.131551
218. M. Yusuf, P. Rosha, F. Qureshi, F.M. Ali and H. Ibrahim, *Sustainable Mater. Technol.*, **43**, e01332 (2025); https://doi.org/10.1016/j.susmat.2025.e01332
219. M. Sathishkumar, M. Saroja, M. Venkatachalam, P. Gowthaman, S. Kannan and A. Balamurugan, *Mater. Lett.*, **323**, 132534 (2022); https://doi.org/10.1016/j.matlet.2022.132534
220. M.C. Maaß, A. Tasch, C. Jooss and T. Waitz, *J. Chem. Educ.*, **99**, 2086 (2022); https://doi.org/10.1021/acs.jchemed.1c01157
221. Y. Piña-Pérez, O. Aguilar-Martínez, C.E. Santolalla-Vargas, Á. Mantilla, E. Samaniego-Benítez, F. González, F. Tzompantzi and V. Santes, *ChemistrySelect*, **9**, e202402184 (2024); https://doi.org/10.1002/slct.202402184
222. Y. Zhi, Y. Yi, C. Deng, Q. Zhang, S. Yang and F. Peng, *ChemSusChem*, **15**, e202200860 (2022); https://doi.org/10.1002/cssc.202200860
223. S. Yu, X.B. Fan, X. Wang, J. Li, Q. Zhang, A. Xia, S. Wei, L.-Z. Wu, Y. Zhou and G.R. Patzke, *Nat. Commun.*, **9**, 4009 (2018); https://doi.org/10.1038/s41467-018-06294-y
224. A.K. Mourya, R.P. Singh, M. Amin, S.R. Barad, M. Abedi and A.V. Wankhade, *Renew. Energy*, **249**, 123166 (2025); https://doi.org/10.1016/j.renene.2025.123166
225. K.A. Gomari, H.Y. Hafeez, J. Mohammed, U.M. Dankawu, C.E. Ndikilar and A.B. Suleiman, *Int. J. Hydrogen Energy*, **200**, 152787 (2026); https://doi.org/10.1016/j.ijhydene.2025.152787
226. S. Gao, Y. Lu, T. Ma, H. Liu and J. Zhang, *Inorganics*, **13**, 166 (2025); https://doi.org/10.3390/inorganics13050166
227. C.I. Rocabruno-Valdés, A. Hernández-Gordillo, R.A. Salinas, G. Santana, V. Rodríguez-González, M. Bizarro and S.E. Rodil, *Int. J. Hydrogen Energy*, **174**, 151285 (2025); https://doi.org/10.1016/j.ijhydene.2025.151285
228. K. He, *Int. J. Hydrogen Energy*, **51**, 30 (2024); https://doi.org/10.1016/j.ijhydene.2023.08.050

229. Y. Piña-Pérez, O. Aguilar-Martínez, P. Acevedo-Peña, C.E. Santolalla-Vargas, S. Oros-Ruíz, F. Galindo-Hernández, F. Tzompantzi and R. Gómez, *Appl. Catal. B: Environ.*, **230**, 125 (2018); https://doi.org/10.1016/j.apcatb.2018.02.047
230. H. Ren, K. Ye, H. Chen, F. Wang, Y. Hu, Q. Shi, H. Yu, R. Lv and M. Chen, *Colloids Surf. A Physicochem. Eng. Asp.*, **652**, 129844 (2022); https://doi.org/10.1016/j.colsurfa.2022.129844
231. L.P. Bao, Y.J. Dong, C.H. Dai, G.D. Xu, Y. Yang, X. Liu, D.W. Ma, Y. Jia and C. Zeng, *Inorg. Chem.*, **60**, 15712 (2021); https://doi.org/10.1021/acs.inorgchem.1c02394
232. X. Xu, J. Zhang, S. Wang, Z. Yao, H. Wu, L. Shi, Y. Yin, S. Wang and H. Sun, *J. Colloid Interface Sci.*, **555**, 22 (2019); https://doi.org/10.1016/j.jcis.2019.07.066
233. S. Kim, Y. Jung, S. So, Y. Kim, S. Seo, J.-C. Park, D.-Y. Kim, J.-H. Lee and S. Lee, *Int. J. Hydrogen Energy*, **127**, 384 (2025); https://doi.org/10.1016/j.ijhydene.2025.04.174
234. C. Chen, X. Deng and Y. Huang, *Surf. Interfaces*, **64**, 106264 (2025); https://doi.org/10.1016/j.surfin.2025.106264
235. Y. Piña-Pérez, E. Samaniego-Benítez, J.H. Sierra-Uribe, F. González, F. Tzompantzi, L. Lartundo-Rojas and A. Mantilla, *J. Environ. Chem. Eng.*, **11**, 109760 (2023); https://doi.org/10.1016/j.jece.2023.109760
236. S. Han, Q. Mao, M. Guo, J. Feng, Y. Xu and Y. Sun, *Ceram. Int.*, **51**, 6422 (2025); https://doi.org/10.1016/j.ceramint.2024.12.086
237. W. Zhang, Y. Xu, Y. Wang, X. Wu, X. Liu, F. Guo, Q. Wu, C. Li and M. Chen, *ACS Appl. Nano Mater.*, **7**, 21993 (2024); https://doi.org/10.1021/acsanm.4c04005
238. F. Ma, X. Xu, C. Huo, C. Sun, Q. Li, Z. Yin and S. Cao, *Inorg. Chem.*, **63**, 8782 (2024); https://doi.org/10.1021/acs.inorgchem.4c00481
239. Y. Zhang, Y. Zhang, Q. Deng, G. Kuang and R. Lin, *J. Energy Storage*, **81**, 110483 (2024); https://doi.org/10.1016/j.est.2024.110483
240. M. Shabbir, R. Akram, S. Javed, Z. Abbas, A. Zafar, S. Mehboob, S. Karim, L. Ali, S. Ali, I. Shakir, A. Nisar and M. Ahmad, *Mater. Adv.*, **7**, 436 (2026); https://doi.org/10.1039/D5MA00889A
241. H. Jiang, Y. Zeng, J. Zhang, Y. Chen, H. Guo, L. Li and Y. Zhang, *Nanotechnology*, **33**, 455402 (2022); https://doi.org/10.1088/1361-6528/ac84e1
242. Y. Jin, H. Seong, J.H. Moon, S.Y. Lee, S.K. Kim, M.H. Yang, J.B. Lee, S.Y. Cho and J. Choi, *J. Alloys Compd.*, **943**, 169076 (2023); https://doi.org/10.1016/j.jallcom.2023.169076
243. R. Zhu, X. Tao, Z. He, L. Yu, T. Wei, H. Xie, J. Xie, P. Li, K. Yu, J. Li, H. Jin, S. Wang and J. Wang, *ChemSusChem*, **18**, e202501774 (2025); https://doi.org/10.1002/cssc.202501774
244. L. Wang, R. Chen, X. Liang, L. Hu, C. Deng, D. Liang, S. Liang and L. Liu, *Nanotechnology*, **34**, 315404 (2023); https://doi.org/10.1088/1361-6528/acd122
245. I. Hussain, D. Mohapatra, G. Dhakal, C. Lamiel, M.S. Sayed, S. Sahoo, S.G. Mohamed, J.S. Kim, Y.R. Lee and J.-J. Shim, *J. Energy Storage*, **36**, 102408 (2021); https://doi.org/10.1016/j.est.2021.102408
246. S.M. Mane, K.S. Wagh, A.M. Teli, S.A. Beknalkar, J.C. Shin and J. Lee, *Micromachines*, **15**, 251 (2024); https://doi.org/10.3390/mi15020251
247. O. Aydin, B. Birol and M. Gencten, *Ionics*, **29**, 3335 (2023); https://doi.org/10.1007/s11581-023-05018-7
248. M. Arif, J. Riaz, A. Bibi, H. Yang and T. Zhu, *APL Mater.*, **12**, 071119 (2024); https://doi.org/10.1063/5.0221353
249. A. Romero-Contreras, L. Garza-Tovar, A. Hernández-Gordillo, L. Cerezo-Durán, E. González-Juárez and E.M. Sánchez-Cervantes, *J. Mater. Sci. Mater. Electron.*, **36**, 722 (2025); https://doi.org/10.1007/s10854-025-14739-6
250. Q. Yu, H. Li, Y. Wen, C. Xu, S. Qin, Y. Kuang, H. Zhou and Z. Huang, *N. Carbon Mater.*, **38**, 543 (2023); https://doi.org/10.1016/S1872-5805(23)60726-7
251. H. Li, J. Wang, Y. Zhao and T. Tan, *Energies*, **11**, 2117 (2018); https://doi.org/10.3390/en11082117
252. M. Haque, I. Konthoujam, S. Lyndem, S. Koley, K. Aguan and A.S. Roy, *J. Mater. Chem. B*, **11**, 1998 (2023); https://doi.org/10.1039/D2TB02265F
253. L.-X. Shan, Y. Li, R.-C. Wang and X.-X. Lian, *J. Alloys Compd.*, **944**, 169223 (2023); https://doi.org/10.1016/j.jallcom.2023.169223
254. L. Tian, Z. Huang, X. Lu, T. Wang, W. Cheng, H. Yang, T. Huang, T. Li and Z. Li, *Inorg. Chem.*, **62**, 1659 (2023); https://doi.org/10.1021/acs.inorgchem.2c04092
255. P. Wu, J. Zhang, S. Wang, A. Zhu and X. Hou, *Chem. Eur. J.*, **20**, 952 (2014); https://doi.org/10.1002/chem.201303753
256. S. Javaheri, F. Keshavarzi and C. Karami, *Sci. Rep.*, **15**, 10717 (2025); https://doi.org/10.1038/s41598-025-90137-6
257. H. Huang, Z. Pan, J. Wang, T. Wang, H. Yu, F. Li, X. Dong, Y. Yang and X. Bai, *Sens. Actuators B Chem.*, **451**, 139422 (2026); https://doi.org/10.1016/j.snb.2025.139422
258. S.K. Ali, W.M. Alamier, N. Hasan, S. Ahmed, A. Ansari and M. Imran, *Appl. Phys., A Mater. Sci. Process.*, **129**, 859 (2023); https://doi.org/10.1007/s00339-023-07124-9
259. F.K. Egualle, A.F. Baye and H. Kim, *Sustainable Mater. Technol.*, **47**, e01858 (2026); https://doi.org/10.1016/j.susmat.2026.e01858
260. Y. Zhao, N. Peng, W. Gao, F. Hu, C. Zhang and X. Wei, *Biosensors*, **14**, 488 (2024); https://doi.org/10.3390/bios14100488
261. Q. Li, F. Li, P. Li and S. Yu, *Ceram. Int.*, **51**, 48935 (2025); https://doi.org/10.1016/j.ceramint.2025.08.227
262. U. Latief, M.S. Khan, S.U. Islam, Z. Khan and M.A. Saifee, *J. Photochem. Photobiol. Chem.*, **445**, 115038 (2023); https://doi.org/10.1016/j.jphotochem.2023.115038